Recent developments in high-moment electroplated materials for recording heads

E. I. Cooper
C. Bonhôte
J. Heidmann
Y. Hsu
P. Kern
J. W. Lam
M. Ramasubramanian
N. Robertson
L. T. Romankiw
H. Xu

The continuous and rapid increase of areal density in magnetic data storage systems required a continuous increase of the coercivity of the storage media. In order to be able to record on these ever-higher-coercivity media, new soft magnetic materials for pole tips with increased magnetic moment had to be developed. Significant progress has been made during the last few years in electroplating alloys with high saturation magnetic flux density for use in writing heads. We review recent progress made in this area, with particular emphasis on the work done at IBM since the review paper on the subject was published in this journal in 1998 by Andricacos and Robertson. Reviewed here are the high-moment alloys of NiFe, particularly in the very high iron range [an extension of permalloy ($Ni_{80}Fe_{20}$) and $Ni_{45}Fe_{55}$]; very-high-cobalt CoFeCu alloys; ternary CoNiFe; and binary iron-rich CoFe alloys. With the latter binary alloy films, we have demonstrated that it is possible to reach by electroplating the saturation flux density limit of 2.4–2.5 T reported for cast alloys. Since the electroplating of good-magnetic-quality iron-rich CoFe alloys posed a considerable challenge, the behavior of the CoFe plating system was studied in detail, using in situ surface pH measurements and a rotating-cylinder Hull cell.

1. Introduction

Hard disk drives are highly complex magnetic storage devices. Their most essential parts are the magnetic medium, which retains the recorded information, and the "head," which is the device that performs the reading and writing processes. The head flies at high speed over the magnetic medium while magnetizing small portions of the medium during the writing process and sensing the local magnetization discontinuities or reversals in the medium during the reading process. The writing process forms "bits," ultrasmall portions of medium uniformly magnetized in one of two opposite directions which are equivalent to the "1" and "0" of the binary code used in digital systems. Detailed descriptions of the structure and mode of operation of magnetic heads, as well as of the magnetic principles and properties relevant to magnetic recordings, can be found in many references, e.g. [1–3]. To increase storage capacity, the areal density (i.e., the number of bits per area of medium, expressed in bits per square inch) must increase, and thus the bit size must decrease. As this happens, the bit will reach a limit at which it becomes thermally unstable; this size, which is a strong function of the medium coercivity, is called the *superparamagnetic limit*.

Higher-coercivity media have had to be developed over time in order to allow smaller bits to be stable. As a consequence, the magnetic flux from the writer has had to increase in order to be able to switch the higher-coercivity bits. One key way to increase write-head pole magnetic flux has been to use materials with ever-higher magnetic moment. The invention and development of such materials and their processing is the subject of this review.

0018-8646/05/$5.00 © 2005 IBM

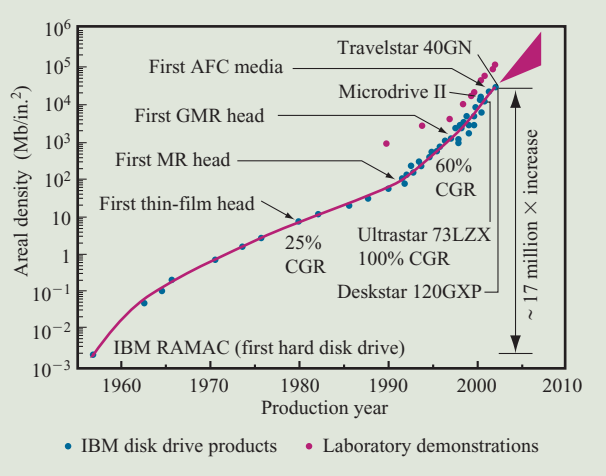

Figure 1

Evolution of the areal density of hard disk drive technology (red – laboratory demonstrations; blue – products). (CGR: yearly compound growth rate.)

Figure 1 represents the eight orders of magnitude increase in areal density achieved over a period of 47 years. It illustrates the strong dependence of the increase of the areal density of magnetic recording on hard disks on the structure and performance of the magnetic recording heads. The different technologies that were implemented in order to sustain this areal density growth rate are represented in Figure 1: thin-film head technology [4–6], magnetoresistive (MR) read head technology [7–9], giant magnetoresistive (GMR) head technology [10, 11], and antiferromagnetically coupled (AFC) media technology [12]. The progress in the electroplating of high-moment magnetic materials, as detailed below, contributed greatly to the implementation of these technologies.

This review paper summarizes the accomplishments of the IBM Thomas J. Watson Research Center and the IBM Storage Technology Division until December 2002 in work that is being continued by Hitachi GST. Since January 2003, the former IBM Storage Technology Division has become a subsidiary company of Hitachi Ltd. Japan, known as Hitachi Global Storage Technologies or HitachiGST, with its headquarters located in San Jose, California.

The realization of the thin-film head technology was possible because of the invention of the appropriate electroplating baths, controls [13, 14], tools [15], and fabrication processes [16–19] for the heads at the IBM Thomas J. Watson Research Center.

In the first generation of recording heads, the plated inductive head acted as both the write and the read element; plated permalloy [an alloy of approximately $Ni_{80}Fe_{20}$ composition and saturation flux density, B_s, of 1.0 tesla (T)] was selected for this purpose because it could meet the stringent material requirements for both reading and writing processes [4]. In fact, compared with writing, inductive reading requires much better magnetic anisotropy, much smaller coercivity [$H_c < 0.5$ oersted (Oe)], low internal stress, and extremely low magnetostriction (λ_s). It quickly became apparent that trying to optimize the material for improved readability was degrading the writability, and vice versa.

Fortunately, the introduction of the magnetoresistive (MR) read sensor [7] combined with the inductive write head [8, 9] led to the physical separation of the writer and the reader that permitted the independent optimization of the reading and writing processes. It allowed the soft magnetic property requirements of the inductive writer material to be relaxed—in particular, increasing the saturation flux density so as to be able to write in higher-coercivity media. A 70% higher magnetic moment was achieved by increasing the iron content from permalloy composition to 55 wt.% iron [20]. Although the values of some of its soft magnetic properties were not as low as in permalloy (e.g., magnetostriction, coercivity), the $Ni_{45}Fe_{55}$ alloy proved to be very successful and was adopted as a standard in the thin-film head industry after permalloy. This paper focuses on the materials that have been investigated at the IBM Thomas J. Watson Research Center and the IBM Storage Technology Division (later HitachiGST) following permalloy and $Ni_{45}Fe_{55}$.

Chronologically, high-cobalt (>75% Co) CoFeCu ternary alloys with a saturation flux density of up to 2.0 T were developed [21–23] as zero-magnetostriction alternatives to $Ni_{45}Fe_{55}$, but they were never implemented in manufacturing. The main reasons for this were weaker corrosion resistance compared with $Ni_{45}Fe_{55}$ and challenges of process control involving deposition of a ternary alloy of uniform composition from a bath containing a very low concentration of a diffusion-controlled element (Cu). The decision not to implement was also motivated by the lack of a conclusive advantage in terms of head performance of CoFeCu compared with $Ni_{45}Fe_{55}$. CoFeCu alloys and their properties are discussed further in Section 3.

The search for platable higher-moment materials was then extended to other regions of the CoNiFe ternary phase diagram (**Figure 2**). CoNiFe ternary alloys were investigated over a large range of composition in parallel with higher-iron NiFe binary alloys [20, 24]. Although CoNiFe alloys exhibited lower values of internal stress and magnetostriction than high-iron NiFe binary alloys, relatively poor corrosion properties and more difficult process control for the former (ternary vs. binary system)

gave an advantage to the high-iron NiFe alloys, of which $Ni_{32}Fe_{68}$ (2.0 T) and $Ni_{20}Fe_{80}$ (2.2 T) were successfully implemented in manufacturing [24]. CoNiFe alloys were intensively studied by universities and by other hard disk drive companies, e.g. [25–27], which led to their implementation in thin-film head manufacturing in numerous companies. High-iron NiFe binary alloys and CoNiFe ternary alloys are presented respectively in Section 2 and Section 4 of this paper.

Finally, in order to reach the highest saturation flux density of the iron-group alloys, i.e., 2.4 T [28], CoFe binary alloys were investigated. In Section 5 this review presents an initial study of the electrodeposition of CoFe alloys without additives. This initial unsuccessful attempt led to the development of a CoFe bath with an additive that allowed plated CoFe binary alloys with B_s of at least 2.4 T to be obtained for the first time [29]. The alloy composition range that exhibited 2.4 T was between 50 wt.% and 70 wt.% iron. The soft magnetic properties and the physical properties of these 2.4-T CoFe alloys are described in Section 6.

The successful plating of alloys with $B_s \geq 2.4$ T prompted studies of their electrodeposition process, in particular the effect of the bath components on the surface pH during plating [30]. The parallel use of a rotating-cylinder Hull (RCH) [31] cell allowed correlations to be made with the studies on the surface pH, in particular the effects of current density and hydrodynamic conditions. These studies helped to optimize the bath composition and plating conditions. The cathode pH and RCH cell studies are presented in Section 7.

Plated CoFe alloys with $B_s \geq 2.4$ T, such as those described in Section 6, do not exhibit ideal material properties; the magnetostriction is very positive (up to +45 ppm) and the internal stress is very high (up to 850 MPa). Such characteristics can strongly affect the magnetic domain structure. This is why a study on domain control in high-moment materials is presented in Section 8.

2. NiFe-based magnetic alloys

The binary NiFe alloys are one group of high-moment materials that have received continuous attention since the early days of magnetic recording. Permalloy ($Ni_{81}Fe_{19}$), with a saturation flux density, B_s, of 1.0 T [3], was historically used as the magnetic material of choice for thin-film cores. It has very desirable attributes; for example, it can be plated into thick films with soft magnetic properties and zero magnetostriction. With its high nickel content, it is also corrosion-resistant. It was used in inductive read–write heads and in the first generations of inductive write–magnetoresistive read heads. As the areal density of drives increased, the need

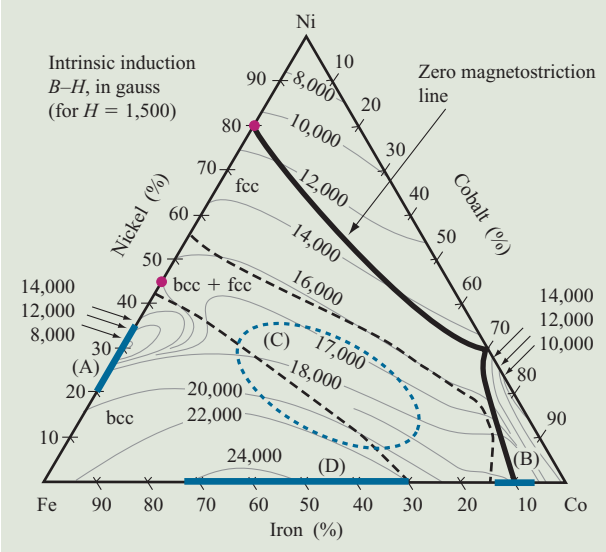

Figure 2

Saturation flux density values (approximate) of annealed bulk CoNiFe alloys as reported by R. M. Bozorth [28]. The following added annotations represent materials discussed in this paper: red symbols – $Ni_{80}Fe_{20}$ and $Ni_{45}Fe_{55}$ alloys; blue lines – (A) high-iron NiFe alloys; (B) CoFe (+Cu) alloys; (C) CoNiFe alloys (all regions); (D) CoFe alloys. Black dotted lines separate fcc, bcc, and fcc–bcc mixed-phase regions. Reproduced from [28] with permission.

for higher-moment materials led to more exploration of the higher-iron, higher-moment binary NiFe alloys. These materials had the potential positive aspects of soft magnetic properties, higher moment, higher resistivity, and good corrosion properties compared with the alternate Co-based high-moment alloys. However, they did have high positive magnetostriction. For the implementation of the alloy $Ni_{45}Fe_{55}$, a robust plating system was developed and the head design was optimized to deal with the positive magnetostriction; as a result, considerably improved drive performance was achieved, with a gain of 70% in moment [20]. This material became a standard in the thin-film head industry after that work.

However, increasing recording densities required the development of materials with an even higher magnetic moment. In order to obtain acceptable films with B_s close to 2.0 T, one must operate on different areas of the Co–Ni–Fe ternary diagram reported by Bozorth [28]. The Co-based ternary alloy systems would be more complex to manufacture and more susceptible to corrosion than the currently popular NiFe system. For bulk alloys, the magnetic moment vs. composition for binary NiFe alloys increases monotonically with increasing iron content up to a composition of 65% Fe, only to decrease to a minimum at 70% Fe and subsequently recover at 80% Fe [28]. However, magnetic properties of electrodeposited

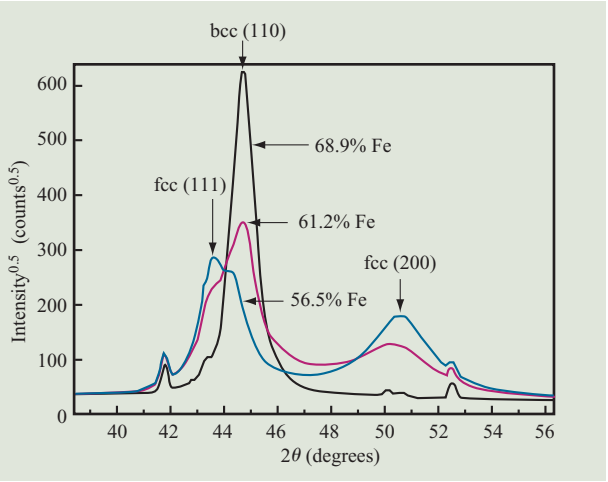

Figure 3

X-ray diffraction patterns for films with different NiFe compositions. (Note that the intensity is plotted as its square root.) θ = diffraction angle. From [24], reproduced by permission of The Electrochemical Society, Inc.

films have been known to vary significantly from bulk alloys that are annealed at extremely high temperatures. Hence, further work was done in order to investigate the magnetic and electrical properties of electrodeposited binary NiFe alloys with compositions ranging from $Ni_{35}Fe_{65}$ through $Ni_{15}Fe_{85}$ [24].

Electrodeposition of these higher-iron NiFe alloys was performed using a sulfate/chloride bath containing boric acid, saccharin, and a surfactant, in a paddle cell [15] in the presence of a magnetic field of ~800 Oe. Temperature was varied between 15 and 30°C, pH between 2.0 and 3.5, and current density between 5 and 20 mA/cm^2. Most films underwent thermal annealing (225°C for 8 hr). They were examined by X-ray fluorescence (XRF) and X-ray diffraction (XRD). Typical properties of these films are shown in **Table 1**.

Further material studies of these films resulted in the X-ray diffraction data shown in **Figure 3**. The alloy undergoes a transition from face-centered-cubic (fcc) structure to fully body-centered-cubic (bcc) structure as the amount of iron is increased in the system. Visual examination of the films plated in the region also showed that the plated film was significantly rougher in the composition region, where the area under fcc peaks is less than 50%. However, at compositions in which the film is essentially single-phase bcc (>67% Fe), the films begin to regain their customary smooth and shiny appearance. This phase change for electrodeposited films correlates very well with the data on bulk materials from Bozorth [28]. However, the composition range in which the phase change occurs is significantly narrower (61–67% Fe) for the plated films than for bulk alloys (65–80% Fe). Thus, it can be seen from Figure 3 that for a 68.9% Fe film, the residual fcc phase content is less than 1% of its content in the 56.5% Fe film. It is noteworthy that the presence of some fcc phase in a mostly bcc mixture does not seem to confer any advantage in the case of NiFe alloys, in contrast to CoNiFe alloys.

The alloy compositions containing ≥68% iron are especially desirable because of their higher moment, which has been shown to result in substantially better overwriting capability in thin-film write heads when compared with material with B_s of 1.7 T ($Ni_{45}Fe_{55}$). At ≥73% iron, an advantageous trend toward lower magnetostriction and higher resistivity also develops. To plate these high-iron alloys, considerably more iron must be placed in the bath, in particular for the highest iron contents, since the anomalous codeposition phenomenon typical of traditional NiFe compositions becomes much weaker here [24]. This fact creates challenges in dealing with ferric ion formation and subsequent hydroxide formation and precipitation. Careful optimization of plating conditions must be done.

In the region of interest, the iron content increases linearly as a function of current density. This is unlike the other NiFe plating baths such as the ones that are used to plate permalloy, in which the iron content as a function of current density goes through a maximum due to mass-transfer limitations at higher current densities. In the present case, the ferrous concentration in solution is significantly higher; therefore, the mass-transfer limitation is not reached at the current densities typically used. Other parameters that can be used to achieve higher

Table 1 Properties of high-moment NiFe films.

Alloy (Ni/Fe wt. ratio)	80/20	45/55	30/70	20/80
Saturation flux density, B_s (T)	1	1.7	2.05	2.2
Post-anneal easy-axis coercivity, H_c (Oe)	0.2	0.5	2	2.5
Post-anneal hard-axis coercivity, $H_{c,h}$ (Oe)	0.01	0.1	1.5	2
Resistivity ($\mu\Omega$-cm)	20	40	30	35
Magnetostriction, λ ($\times 10^{-6}$)	< -3	20	25	25
Stress (MPa)	100	160	225	240

iron content are temperature (lower is better) and pH (lower is better, at least for pH $\geq$2.75). As a result of this study, a robust plating system could be designed for plating $Ni_{20}Fe_{80}$ alloy films.

These very-high-moment NiFe alloys have shown increased performance in disk drives and have become popular in mass production of thin-film heads.

3. CoFeCu

High-cobalt CoFeCu is a soft magnetic alloy that has generated considerable interest. The addition of copper to high-cobalt CoFe refines the grain size, broadens the range in which a mixed fcc/bcc structure is obtained, and thus greatly broadens the scope of compositions for which coercivity is low, while other useful magnetic properties remain within the desired range for writing heads.

Plating of CoFeCu films for magnetic heads was initiated at IBM more than a decade ago (Chang et al. [21, 32, 33], Andricacos and Robertson [34]); other groups have also investigated this material (Ye et al. [35], Kakuno et al. [36], Park and Allen [37], Poupon [38], Gigandet et al. [39]) because of its many attractive properties:

- High saturation flux density, B_s, in the 1.8–2.0-T range.
- Low magnetostriction, $\lambda_s \sim 0$–$\pm 3 \times 10^{-6}$, easily adjustable in magnitude and sign, an important advantage over most other high-moment materials.
- Low coercivity: $H_c < 1$ Oe for most relevant compositions.
- Low internal stress.
- Feasibility of forming a laminated deposit from one bath by modulating the current density [23, 33].

The more recent work at IBM has focused on performance evaluation of plated CoFeCu in write heads, better understanding of process conditions, and improvement of process controls. On the basis of previous results [21, 32, 33], plating was directed primarily at obtaining deposits with 5–12% iron and 6–10% copper. This composition range contains alloys with low H_c and low absolute values of λ_s.

The plating bath and electrodeposition conditions for CoFeCu are detailed elsewhere [22]. A sulfate-based solution was used, buffered by acetic and boric acid and with saccharin as an additive. A horizontal paddle cell [15] was used, with a cobalt anode and a permanent magnet. The solution was recirculated and kept at 25°C and pH 3.00. Films were examined by XRF and by XRD. Magnetic properties were measured from *B*–*H* hysteresis loops.[1] Magnetostriction was determined by bending the film substrate to a hard stop to predetermined deflection values (corresponding to several curvature values) and measuring the resulting change in the value of the magnetic anisotropy field, H_k.

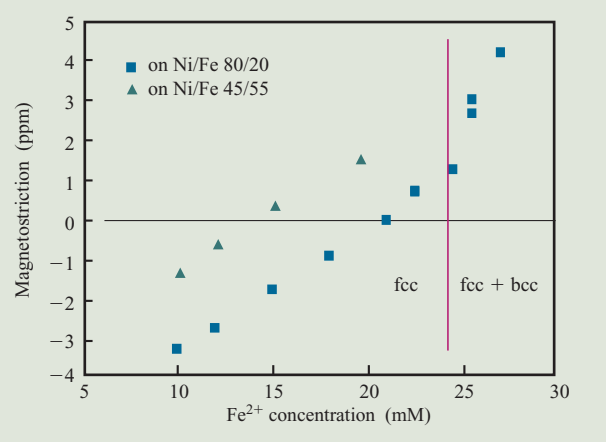

Figure 4

Magnetostriction as a function of Fe^{2+} concentration in the plating solution. The measured values contain a contribution from the seed layer. From [22], reproduced by permission of The Electrochemical Society, Inc.

The low magnetostriction, λ_s, is a major feature of CoFeCu. It was found that an easy way to control the magnitude and sign of λ_s is by varying the Fe^{2+} concentration, $[Fe^{2+}]$ (**Figure 4**), while the coercivity, H_c, stays below 1.2 Oe. Notably, the kink in the λ_s vs. $[Fe^{2+}]$ curve in Figure 4 coincides with a crystal structure change, from nearly pure fcc to fcc and bcc mixed in similar amounts.

Since copper deposition is diffusion-controlled, the copper content of the film varies linearly with $[Cu^{2+}]$ and inversely with current density. Increasing $[Cu^{2+}]$ causes a decrease in λ_s. Copper content has only a diluting (not destructive) effect on the magnetic moment.

Saccharin is used as a grain refiner, to ensure low coercivity and a mirror-bright finish. Its concentration was explored in the range from 0.125 to 42 mM and from pH 2.5 to 4.5. Interestingly, the required saccharin concentration is roughly inversely proportional to the H^+ concentration (e.g., ~1.25 mM needed at pH 3 and ~12.5 mM at pH 4). Saccharin is a medium-strength acid with $pK_a \sim 2$.[2] It is likely therefore that the neutral (protonated) molecule is the cathode-active form of saccharin, while most of the saccharin at pH >2 (and a larger proportion as pH increases) is in its presumably inactive anionic form.

[1] Graphic displays of the magnetic flux density *B* of a sample as a function of a cycled external magnetic field *H*.

[2] pK_a: the negative value of the logarithm of an acidity equilibrium constant.

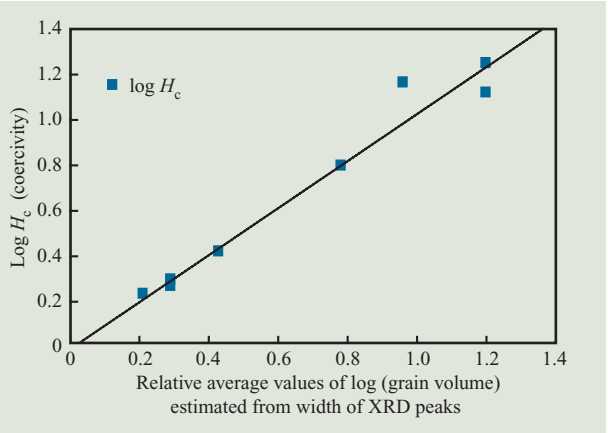

Figure 5

Coercivity as a function of particle size in "slices" plated at different current density values. Note that the slope of the log–log correlation, $y = -0.00739 + 1.04x$, is about 1. From [22], reproduced by permission of The Electrochemical Society, Inc.

The presence of acetic acid is necessary for preventing precipitation of ferric compounds, since acetate anions complex ferric ions while limiting the pH increase near the cathode (see Section 7 for a detailed discussion of this issue in the CoFe case). Surprisingly, acetic acid is also needed for effective saccharin activity. The latter effect is probably also due to buffering (i.e., keeping the pH low near the cathode), which keeps more of the saccharin protonated.

Current density effects were investigated in a Hull-cell-like setup formed by covering most of the anode of the horizontal paddle cell, which was otherwise operated as usual. Patterned wafers or copper sheet cathodes were used as samples; the plated copper sheets were cut into stripes for which *B*–*H* loops and XRD patterns were obtained. Higher current densities (12–18 mA/cm^2) yielded lower grain size and much smoother deposits than lower current densities (3–6 mA/cm^2), both over the copper coils in the head yoke and elsewhere. Interestingly, H_c is roughly proportional to the relative grain volume (**Figure 5**) as calculated from the relative grain size. The latter is estimated from the width at half height of XRD peaks.

The CoFeCu bath is quite easy to control. The main concern is the tendency of cupric ion concentration, [Cu^{2+}], to vary quickly, because of the diffusion-limited electroreduction of Cu^{2+} (copper being the noblest of the three metals), its low concentration (0.25–1 mM), and its exchange reaction with the cobalt anode. Since [Cu^{2+}] strongly affects λ_s, it requires continuous replenishment. A fast (<10 min), precise analytical procedure was therefore developed, based on the formation of the Cu^{+}–neocuproine complex [40]. Reaction, extraction, centrifugation, and colorimetry are all performed consecutively in a test tube, with no interference from the large excess of Co^{2+} and Fe^{2+} ions. This method was used to adjust the replenishment rate and keep [Cu^{2+}] constant to within ±2–3%.

Corrosion rates of CoFeCu are substantially higher than those of $Ni_{45}Fe_{55}$ and much higher than those of permalloy.

Write heads with CoFeCu top yokes and poles were fabricated in the head manufacturing line using the standard process. These heads had permalloy bottom pole tips, 12-turn coils, a stack height of about 5 μm, and a yoke length of about 75 μm. The pole tips were 2.3 μm wide and the write gaps were 0.2 μm long. Three different magnetostriction (λ_s) values (-1×10^{-6}, -2×10^{-6}, and -3×10^{-6}) for the CoFeCu poles were achieved by varying the Co/Fe ratio. A wafer with $Ni_{45}Fe_{55}$ top poles ($\lambda_s = +25 \times 10^{-6}$) was used as the experimental control.

As expected, the low magnetostriction and low stress of CoFeCu confers some advantages on this material in comparison with $Ni_{45}Fe_{55}$. Among these are better domain configuration (see Section 8), more stability against wafer processing effects, better inductance rolloff characteristics, and lower Barkhausen noise.[3] Generally, CoFeCu was found to have an advantage in yoke-dependent properties. However, its recording performance was similar to that of $Ni_{45}Fe_{55}$ for the $\lambda_s = -1 \times 10^{-6}$ sample and slightly inferior for the other two. This result is not consistent with the inductance data.

To elucidate the problem, cross-sectional EDX[4]composition analysis was performed. Substantial compositional variation was found across the length direction of the yoke. In general, the CoFeCu pole tip area was cobalt-rich and copper-deficient compared with the yoke area, while iron content was nearly constant across the device. Since copper promotes the fcc/bcc mixture, the low copper content may lead to high coercivity in the pole tip area, which in turn degrades the high-frequency performance. The composition change along the yoke and pole tip can be explained by the local current density variation, which results from the sharp change of the slope in the topography of the plated material and from local depletion of copper ions in the diffusion layer. This difficulty with composition control is typical of alloy plating systems in which a minor component is diffusion-controlled. The lack of significant high-frequency improvement in performance relative to $Ni_{45}Fe_{55}$ may also be due in part to the low resistivity of CoFeCu, about half that of $Ni_{45}Fe_{55}$.

[3] Noise resulting from irreversible domain wall motion caused by an external magnetic field.
[4] Energy-dispersive X-ray spectroscopy.

4. CoNiFe

Electrodeposited CoNiFe alloys have been the subject of numerous studies in recent years, e.g. [41–43]. In general, these alloys possess excellent soft magnetic properties, and in some cases they exhibit a magnetic moment up to 2.1 T [43]. The first successful attempts at $B_s \geq 2.0$ T were reported by Osaka and coworkers [44, 45]. They found that by avoiding any sulfur-containing additive (such as saccharin or thiourea), the range of stability of the fcc structure was expanded toward compositions richer in iron, thus higher in magnetic moment. They also observed that, near the fcc/bcc boundary, the grain size of the mixed-phase alloy was much smaller; consequently, coercivities were much lower than elsewhere. At the same time, the zero-magnetostriction line in the ternary phase diagram (see Figure 2) was also shifted to the left (i.e., toward a higher percentage of Fe), close to the fcc/bcc boundary. Thus, high B_s, low H_c, and low λ_s could be obtained at the same time.

However, the CoNiFe bath with no sulfur additives had a substantial problem: The high internal stress of the films limited the platable thickness to <1 μm. We tried, therefore, to design a plating process that minimizes film stress while preserving the advantages of Osaka's bath to the extent possible [27].

CoNiFe films were electrodeposited galvanostatically from a sulfate/chloride bath. The bath chemistry was based on the $Ni_{45}Fe_{55}$ plating bath [34], with ammonium and cobalt salts [41–43] added to plate CoNiFe. It contained 0.15–0.2 M $NiSO_4$, 0.02–0.1 M each of $FeSO_4$ and $CoSO_4$, 0.4 M boric acid, 0.18 M NH_4Cl, 0.05 M $(NH_4)_2SO_4$, 25 ppm of specially conditioned saccharin, and 10 ppm of FC-95 surfactant. A large alloy composition range (8–40 wt.% nickel, 28–68 wt.% cobalt, and 10–55 wt.% iron) was achieved by changing the concentrations of Ni^{2+}, Fe^{2+}, and Co^{2+} and by varying the current density between 3.5 and 20 mA/cm^2 while keeping the total charge constant. More than 250 different alloy compositions were deposited. In most cases, the iron and nickel contents of the films were varied by changing only the current density for a given bath composition, as shown in **Figure 6**. The cobalt content of the films was modified by changing the Co^{2+} concentration in the bath.

The substrates—glass samples sputtered with 80 nm of $Ni_{45}Fe_{55}$ seed layer—were plated in a horizontal paddle cell at 27°C and pH 3, in a magnetic field of 700–800 gauss, using a nickel anode (99.9% Ni). Film thickness ranged from 1 to 3 μm depending on current efficiency. Film composition and microstructure were obtained using XRF and XRD, respectively. Magnetic properties were measured with a hysteresis B–H loop tracer ("B–H looper"), and electrical resistivity with a four-point probe. Internal stress values were calculated from sample curvature measured by profilometry before and after plating. All data were measured on as-plated samples.

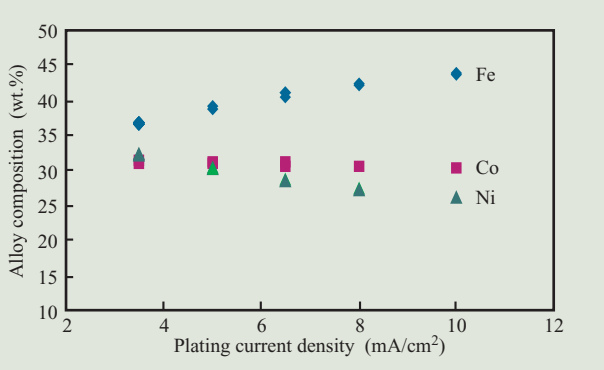

Figure 6

Variation of alloy composition with plating current density for a bath containing 0.2 M nickel sulfate, 0.02 M ferrous sulfate, and 0.03 M cobalt sulfate. From [27], reproduced by permission of The Electrochemical Society, Inc.

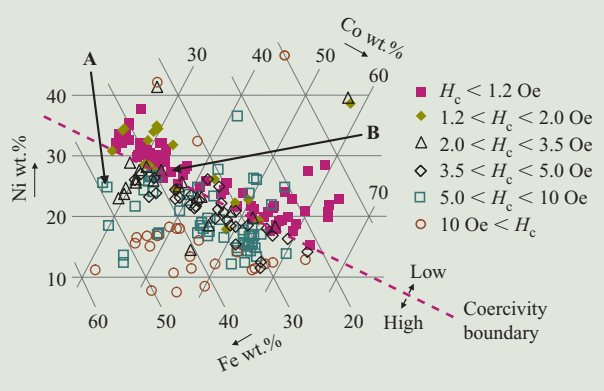

Figure 7

Ternary diagram of electrodeposited CoNiFe alloy showing different easy-axis coercivities. Open symbols: $H_c > 2.0$ Oe; solid symbols: $H_c < 2.0$ Oe. **A** and **B** (arrows) represent two samples with very different easy-axis coercivities chosen for microstructure analysis (see Table 2). From [27], reproduced by permission of The Electrochemical Society, Inc.

CoNiFe: Results and discussion

Figure 7 is a ternary diagram mapping the easy-axis coercivity, H_c, of the CoNiFe films as a function of alloy composition. The data is arranged into groups of similar H_c values. It clearly demonstrates the presence of a region (solid symbols) where H_c values remain very low, i.e., below 2 Oe (as plated). Below this boundary, H_c increases rapidly. In this system, H_c appears to be an intrinsic property of the CoNiFe film, because data shown in Figure 7 has been generated with different applied plating current densities and/or bath compositions. Comparing Figure 7 with corresponding ternary diagrams by Osaka

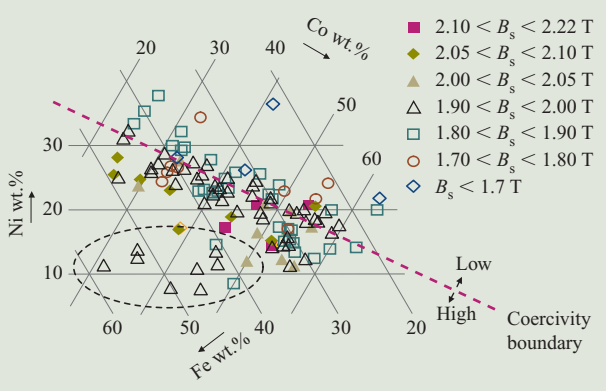

Figure 8

Ternary diagram of electrodeposited CoNiFe alloy showing different magnetic moments. Open symbols: $B_s < 2.0$ T; solid symbols: $B_s > 2.0$ T. The oval indicates a region in which the magnetic moment is expected to be above 2 T on the basis of bulk data [28]. From [27], reproduced by permission of The Electrochemical Society, Inc.

and co-workers [44, 45] reveals that the $H_c < 2$ Oe region here is well to the "south" (i.e., low-Ni direction) of Osaka's $H_c < 2$ Oe region obtained in saccharin-based baths, but slightly to the "north" of his results in the absence of sulfur-containing additives. This is reasonable in view of the low concentration (25 ppm) of additive in our saccharin-based bath. Two samples, A and B, in the high- and low-H_c regions, respectively, were selected for materials analysis (see **Table 2**). The abrupt decrease in H_c observed between sample A (8 Oe) and sample B (0.45 Oe) is clearly correlated to the transition from a fully bcc microstructure to an fcc/bcc-phase mixture. From XRD results, the grain size is about seven times smaller in B, where both phases are present, than in A, which is purely bcc.

Figure 8 is a ternary diagram mapping the saturation flux density, B_s, for all of the CoNiFe films for which it was measured. As in Figure 7 for H_c, B_s data is arranged in groups of similar values. The boundary between low- and high-H_c compositions shown in Figure 7 is reproduced in Figure 8. As a general trend, B_s values increase when iron content increases and nickel content decreases in the alloy. However, in the region represented by the oval, B_s values are lower than expected. On the basis of literature data on bulk alloys [28], this region should consist of very-high-moment CoNiFe. The fact that the brightness of CoNiFe electrodeposits in this region is degraded suggests the incorporation of oxides and hydroxides, which could explain the lower B_s values.

Although very few high-moment samples ($B_s > 2.0$ T) are located in the low-coercivity region, high B_s *and* very low H_c coexist around the alloy composition $Co_{55}Ni_{20}Fe_{25}$. For instance, for a selected sample from this region, $B_s = 2.21$ T, with easy- and hard-axis coercivities of <1 Oe. Such a material is potentially a good candidate for high-performance write heads. Although samples with $B_s > 2.0$ T have been obtained, this CoNiFe plating system suffers from poor reproducibility in the high-moment region, as shown in Figure 8. Better reproducibility is observed for samples with lower B_s, e.g., a typical $Co_{44}Ni_{27}Fe_{29}$ sample with $B_s = 2.0$ T, $H_c = 1.2$ Oe, $\lambda_s = +3.5 \times 10^{-6}$, electrical resistivity of 30 $\mu\Omega$-cm, and a remarkably low internal stress as plated of 115 MPa. In general, the CoNiFe samples had low internal stress, and typical films withstood thermal annealing without structural damage.

Mapping of the magnetic properties of these CoNiFe alloys shows a clear transition boundary where the easy-axis coercivity increases drastically. This transition corresponds to a change from a mixed bcc/fcc phase structure to single-phase bcc. The easy-axis coercivity of CoNiFe alloys is very low (<2 Oe) when mixed phases (bcc/fcc) are present. This finding is consistent with results obtained by other groups.

Most of the plated CoNiFe films presented in this study show a magnetic moment above 2.0 T. The magnetic moment of low-nickel-composition CoNiFe alloys is below what is expected in literature for these alloy compositions. Oxygen incorporation is believed to be the cause. However, CoNiFe films with magnetic moment as high as 2.2 T have been electrodeposited with excellent soft magnetic properties.

5. CoFe—Plating without additives

The CoFe alloy system includes compositions that possess the highest known room-temperature saturation flux density (B_s of about 2.4–2.45 T), in the range of 50 to 70 wt.% iron [28]. Plating good-quality CoFe films may

Table 2 Comparison of crystalline structure, coherence length, and easy-axis coercivity for two selected films with alloy compositions **A** and **B** shown in Figure 7.

Sample	*Fe* (wt.%)	*Co* (wt.%)	*Ni* (wt.%)	*Crystalline structure*	*Grain size* (Å)	*Coercivity* (Oe)
A	48.8	26.2	25	bcc	300	8
B	37.5	35.1	27.4	bcc/fcc	39	0.45

be considered to be the ultimate prize in the pursuit of new high-moment soft magnetic films. Until recently, however, little was published about electroplated alloys of these compositions, especially when compared with NiFe plating or more recently with CoNiFe plating; presumably the reason is the difficulty of plating films with good properties (magnetic, corrosion, internal stress). In addition, for modeling of anomalous codeposition the NiFe system is preferred to CoFe because of its much more distinct anomalous behavior. Moreover, most studies on CoFe plating do not report measurement of soft magnetic properties [47–51]. Following is a short account of previous work on CoFe plating.

The full range of electroplated Co_xFe_{1-x} compositions (x = 1 to 0) was investigated by Kakuno et al. [50] using an additive-free sulfate-based plating bath. The thin films obtained showed heterogeneous morphology and composition and were apparently prone to cracking; thus, they would not be suitable for the fabrication of thin-film heads and other microstructures. Most magnetic properties of these films were never reported.

In U.S. Patent 4,208,254 [52], Mitsumoto et al. disclosed a method of electrodepositing Co_xFe_{1-x} alloys with x (wt. fraction) = 0.925 to 0.45, from a fluoride-containing bath. No indication of values for the saturation flux density was given.

Abd El Rehim et al. [53] described CoFe thin films with compositions ranging from about 43% up to about 66% iron plated from an acetate bath. The deposits had microcracks, and magnetic properties were not reported.

Liu et al. [54] plated CoFe films but concluded that for improved soft magnetic properties the addition of nickel was desirable.

Shao et al. [55] plated thick low-stress CoFe films from a concentrated sulfamate bath. Saturation flux density was $\leq$2.2 T, presumably because of the incorporation of substantial amounts of sulfur, etc. in the deposit.

Recently, Osaka et al. [56] reported 2.0–2.1-T $Co_{35}Fe_{65}$ films plated from a sulfate–NH_4Cl–boric acid bath. They showed that moments approaching theoretical values could be obtained either by adding the reducing agent trimethylamineborane (2.3 T) or, better, by using a dual-cell system with separate anode compartment (2.4 T). The lowest coercivity after optimized annealing was 8 Oe. The authors stressed the importance of preventing oxidation of ferrous to ferric ions in order to maximize the magnetic moment.

In an initial study [57], the IBM group attempted to obtain films with B_s of 2.4 T by plating CoFe containing 48–67 wt.% iron from an additive-free sulfate-based bath. The additive-free route had been shown to be quite successful in the CoNiFe case [41]. In addition to sulfates of Co^{2+} and Fe^{2+}, the bath contained 25 g/L boric acid, 10 g/L NaCl, 1 g/L sodium citrate, and 0.01 g/L surfactant, and in typical runs had a pH of 2.86. The film composition was varied by changing the $CoSO_4$ concentration. Plating was performed in a paddle cell (paddle frequency = 1 Hz) at room temperature, with a cobalt anode, in a 700–800-gauss magnetic field. Current density was typically 7 mA/cm^2, but values up to 28 mA/cm^2 were tried (see below). Alloy composition was measured by XRF; H_c and H_k were measured using a B–H looper; B_s was obtained using a vibrating sample magnetometer (VSM).

The electroplated films were dark in color and developed cracks either on standing or after 240°C/2 hr annealing. The plating rate was low (typically 21 nm/min, current efficiency 14.5%). Easy-axis coercivity, H_c, decreased from 5.8 to 2.6 Oe as the wt.% of iron increased from 48% to 67%. Other properties varied somewhat irregularly: hard-axis coercivity (3.0–5.7 Oe), H_k (18.6–35.7 Oe), B_s (1.87–2.14 T). The highest saturation flux density (2.14 T, substantially less than the expected ~2.4-T value) was obtained for a 49-wt.% iron sample. In addition, the films were magnetically isotropic in the plane of the substrate.

Another problem of the initial series of CoFe samples was high surface roughness ("nodules" as large as 2 μm). It was found that the nodules could be eliminated by a combination of lower plating pH (2.60) and higher current density (14–28 mA/cm^2), but under these conditions pits tended to form, possibly because of increased hydrogen evolution. The pits could be eliminated by pulse plating (1 s on/0.5 s off). More significantly, the higher current density values tended to raise the B_s values. In the best case, at 21 mA/cm^2 a 53-wt.% iron film with B_s = 2.18 T was obtained, compared with 2.07 T for the same composition plated at 7 mA/cm^2 and pH 2.86. Current efficiency was low and very sensitive to current density, ranging from 0.5% at 14 mA/cm^2 to 37% at 28 mA/cm^2. CoFe films up to 3 μm thick were plated without delamination.

Unlike low-iron CoFe films (e.g., $Co_{90}Fe_{10}$ [58]), plated high-Fe-content CoFe films exhibited substantially lower moment than the equivalent bulk materials. The main cause of the failure to reach a B_s value of 2.4 T was probably the massive incorporation, during plating, of oxygen into the deposit; this does not occur during casting of CoFe alloy. The importance of oxygen incorporation was shown by XPS analysis of two typical CoFe films after sputtering away the surface layer. A $Co_{47}Fe_{53}$ film deposited at pH 2.60 and high current density (21 mA/cm^2) contained ~3.5 at.% O and had B_s = 2.18 T. By comparison, a film of similar composition deposited at pH 2.86 and low current density (7 mA/cm^2) contained 7–10 at.% O and had a B_s of only 2.07 T. The lower pH reduces the availability of oxygen-containing

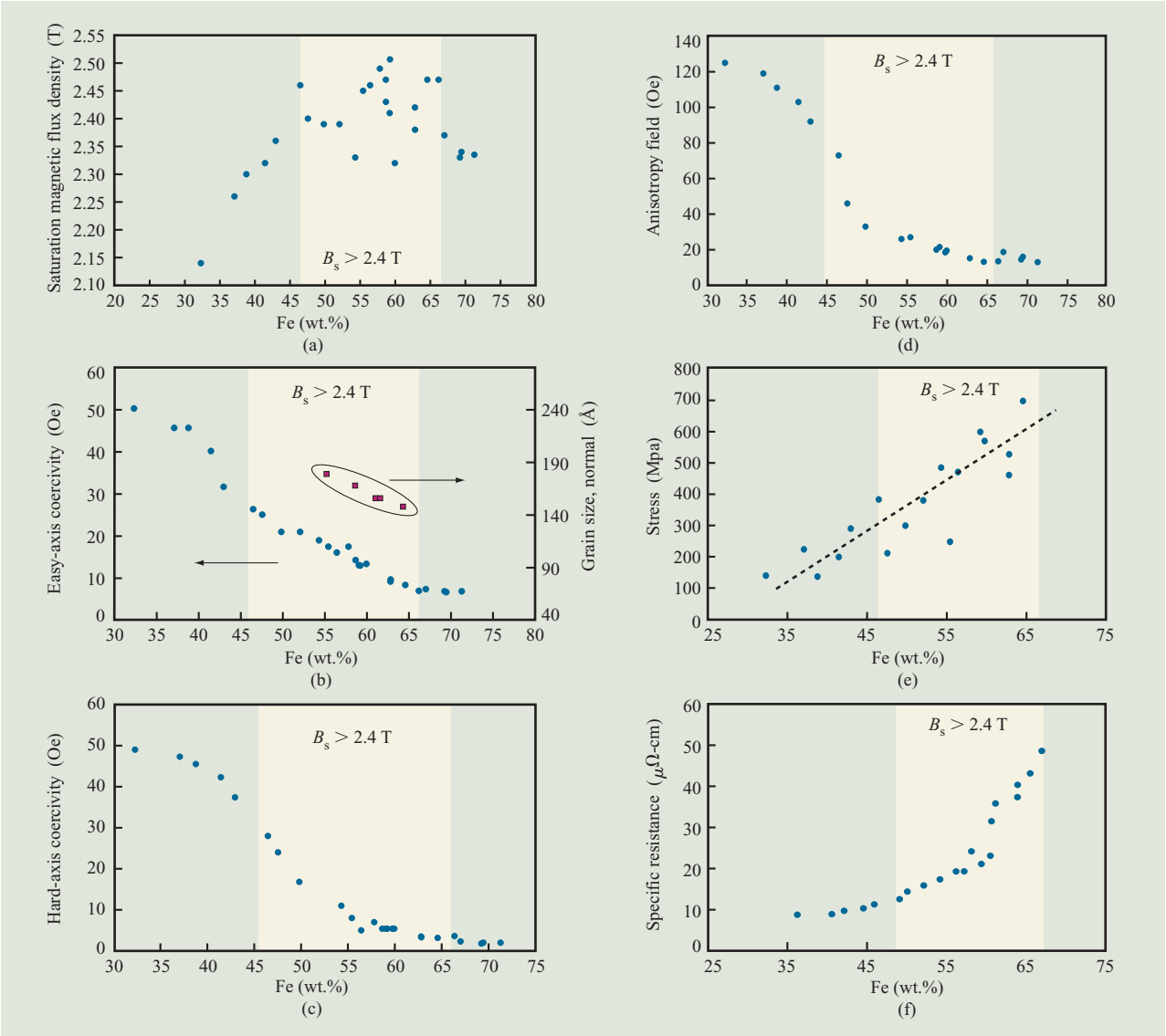

Figure 9

Electroplated CoFe films: (a) Saturation magnetic flux density; (b) easy-axis coercivity and normal-to-plane grain size [46]; (c) hard-axis coercivity; (d) anisotropy field; (e) stress; (f) specific resistance; all as a function of iron content. From [29], reproduced by permission of The Electrochemical Society, Inc.

species near the cathode surface by destabilizing hydrolyzed cations. Since ferric ions are the most important hydrolyzed species at the plating pH, it is likely that $Co_{90}Fe_{10}$ [58] films were closer to bulk properties primarily because the bath from which they were plated had much lower concentrations of iron ions.

Current efficiency for the samples described above was low, a condition that is likely to promote oxygen incorporation. The reason for this is that low current efficiency is accompanied by increased hydrogen evolution, which in turn causes an increase in pH near the cathode and therefore an increase in the local concentration of hydrolyzed species; the net result is that more oxide and/or hydroxide is incorporated into the film. We therefore turned our attention toward finding plating conditions that would substantially increase the current efficiency.

6. Electroplated 2.4-T CoFe films

The problem of lower magnetic moment (max. 2.18 T for $Co_{47}Fe_{53}$) in CoFe thin films electrodeposited in our initial study [57] was shown to be correlated to oxygen

incorporation in the films. Therefore, the bath used there was modified by replacing the citric acid used in low concentration (1 g/L) with acetic acid used in much larger quantity in order to complex ferric ions selectively and to provide more effective buffering action, and by the addition of a sulfur-containing additive.

In the modified method [29], CoFe films were galvanostatically electrodeposited from a sulfate-based bath containing cobalt and ferrous sulfates, sodium chloride, boric acid, acetic acid, a surfactant, and a proprietary organic sulfur-bearing additive (SBA) which replaced the commonly used saccharin. Electrodeposition was performed on glass samples sputtered with 80 nm of $Ni_{45}Fe_{55}$ seed layer, in a horizontal paddle cell equipped with a pure cobalt anode (99.95% Co), at room temperature, pH 3.00, and in a magnetic field of 700–800 gauss. Alloy composition was varied by changing the Fe/Co ratio in the bath and by adjusting the plating current density within a range of 5–20 mA/cm^2. Film alloy composition and microstructure were respectively obtained using XRF and XRD. Oxygen content was measured using Auger electron spectroscopy (AES) depth profiling. Magnetic properties were measured using a *B–H* looper, electrical resistivity using a four-point probe. Internal stress values were calculated on the basis of profilometry measurements done before and after plating.

The result of the bath changes was dramatic, as can be seen in **Figure 9(a)**, in which the magnetic moment is represented as a function of the iron content. The magnetic moment B_s of CoFe films in the composition range of ~46 wt.% Fe to ~66 wt.% Fe is at least 2.4 T. It is represented in Figures 9(a)–9(f) by a shaded region.

In **Figures 9(b)** and **9(c)**, which represent respectively the easy-axis and hard-axis coercivities of CoFe as a function of alloy composition, it can be observed that both coercivities decrease as iron content increases, although the hard-axis coercivity decrease is much more pronounced in the first half of the 2.4-T composition range. The decrease of coercivity with increasing iron content is related to a decrease in grain size, as shown in Figure 9(b). **Figure 9(d)** shows that the anisotropy field of CoFe films is fairly stable around 20–30 Oe above ~55 wt.% Fe. Up to ~55 wt.% Fe, the decrease of the anistropy field with higher wt.% iron is very substantial. In **Figure 9(e)**, notwithstanding the large scatter (which is attributed to the measurement technique), the internal stress of the CoFe films is seen to increase markedly with the iron content. Finally, **Figure 9(f)** shows that the electrical resistivity of the CoFe films increases rapidly within the 2.4-T region.

Table 3 summarizes the properties of a typical $Co_{38}Fe_{62}$ film as plated and after annealing at 200°C for 11 hours. The saturation flux density is not degraded upon annealing, and low easy- and hard-axis coercivities of respectively ~5 Oe (compare with 8 Oe in [56]) and ~2 Oe are observed upon annealing. The internal stress in alloys around this composition is fairly high as plated, and it goes up after annealing. A maximum plated thickness of 1.7 μm was reached when plating on glass substrates sputtered with $Ni_{45}Fe_{55}$ seed layer. The magnetostriction of $Co_{38}Fe_{62}$ films is positive and high, similar to the values for bulk CoFe at comparable alloy composition.

Table 3 Summary of soft magnetic properties and physical properties for $Co_{38}Fe_{62}$.

Properties	*As plated*	*After annealing at 200°C for 11 hours*
Saturation flux density, B_s (T)	2.48	2.48
Easy-axis coercivity, H_c (Oe)	13	5.3
Hard-axis coercivity, $H_{c,h}$ (Oe)	4.8	2.3
Anisotropy, H_k	20.1	20.1
Stress (MP_a)	625	845
Magnetostriction, λ	$+ 45 \times 10^{-6}$	N/A

In addition, XRD data shows that such a $Co_{38}Fe_{62}$ film is purely bcc-phase with a (110) preferred orientation and, according to AES depth profile, has a bulk oxygen concentration of <0.5 at.%. This is a very low value compared with the 3.5–10 at.% of oxygen present in CoFe films prepared in our initial study (see Section 5), and would explain why the magnetic moment of the CoFe films there was at most 2.18 T, vs. 2.4 T for bulk alloys of similar composition (Figure 2). The low oxygen level in the CoFe films fabricated by the modified method is attributed to the bath chemistry changes, particularly the addition of SBA.

The ideal material for a recording head should have the highest moment, the lowest coercivities (easy/hard axis), zero magnetostriction, very high electrical resistance, no internal stress, and very high corrosion resistance. Although such a material does not exist, one can choose an optimal alloy composition determined by the most important properties for a particular head (e.g., pole tip material vs. yoke material). Compromises must be made, though fortunately a broad range of high-moment compositions is available to choose from. For instance, a high iron content would be favorable for lowering coercivities and increasing resistivity, but a lower iron content would be favorable for stress reduction; the optimal value depends in part on the designed thickness of the CoFe layer, since stress is a strong function of thickness. Similar considerations apply to other properties such as magnetostriction or corrosion resistance. Many of these material properties are not intrinsic, and more learning is needed in order to change

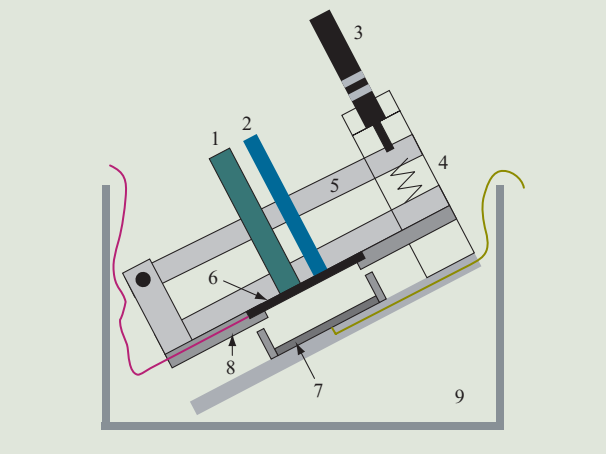

Figure 10

Schematic of surface pH cell: (1) flat-bottomed pH electrode; (2) SME reference electrode; (3) micrometer; (4) spring; (5) movable arm; (6) metal screen (cathode); (7) anode (platinum); (8) cover plate; (9) container with CoFe plating solution. From [31], reproduced by permission of The Electrochemical Society, Inc.

them independently of the alloy composition and, to the extent possible, of one another.

7. CoFe—Cathode pH and RCH cell study

The success in plating the first good-quality CoFe films with $B_s \geq 2.4$ T [29], as opposed to the lower-moment, dark films obtained earlier [57] led to many questions concerning the role of the various solution components, the differences between the CoFe plating system and other iron group systems discussed above, and the ways to achieve optimal operating conditions. A more thorough understanding of CoFe electrodeposition was in order. Two powerful methods—*in situ* surface pH measurements and the rotating-cylinder Hull cell (RCH cell)—were employed for this purpose. The following account summarizes a more comprehensive study [31].

Most transition metals and alloys are deposited with simultaneous evolution of hydrogen. This is accompanied by a rise in pH near the cathode, which can significantly exceed the bulk pH and affect the chemistry and reactivity of nearby ions as well as the stability of intermediate products [59]. Measurements of pH at the surface during plating [30, 60, 61] help us to understand the mechanisms of alloy deposition. For example, in plating of CoFe alloys, it is essential to keep the surface pH, during plating, below the limit at which oxides and hydroxides are precipitated and trapped in the deposits. As pointed out above, incorporated oxides lower the magnetic moment; they also lead to structural defects.

The thermodynamic stability of hydroxides is usually expressed in Pourbaix diagrams [62]. These diagrams show the window of hydroxide stability as a function of potential and pH. More recently, hydrolysis of cations and the stability of hydroxides have been discussed in detail by Baes and Mesmer [59]. Below pH ~7, ferrous hydroxide species are thermodynamically unstable. However, the ferric ion is partially hydrolyzed even at pH 1 [59] according to the following reaction:

$$x\mathrm{Fe}^{3+} + y\mathrm{H_2O} = \mathrm{Fe}_x(\mathrm{OH})_y^{(3x-y)+} + y\mathrm{H}^+. \quad (1)$$

In acidic solutions, the two mononuclear ferric species FeOH^{2+} and $\mathrm{Fe(OH)}_2^+$ as well as the dinuclear species $\mathrm{Fe_2(OH)}_2^{4+}$ are formed, with $\mathrm{Fe(OH)}_2^+$ appearing at a pH of around 3. $\mathrm{Fe(OH)_3}$ (aq) and $\mathrm{Fe(OH)}^{4-}$ appear only in neutral and basic media, while the amorphous precipitate of $\mathrm{Fe(OH)_3}$ crystallizes into α-FeO(OH) in the presence of ferrous ions [59]. According to Figure 10.13 in Baes and Mesmer [59], the solubility of α-FeO(OH) decreases rapidly with increasing pH, being approximately 100 times larger at pH 3 than at pH 4. Knowing the cathode pH during plating and avoiding conditions in which hydroxides precipitate at the cathode are therefore crucial in order to obtain high-quality CoFe films.

In situ surface pH measurements

To measure the cathode surface pH during plating, a special cell, identical to one described earlier by Romankiw [30], was built **(Figure 10)**. In the apparatus, a flat-bottomed pH electrode is brought into contact with the back of a very thin metal (e.g., nickel) mesh consisting of small, uniform square apertures. If the thickness of the metal screen is small compared with the diffusion layer thickness of H^+ and if the diameter of the apertures is less than twice the diffusion layer thickness, changes in proton activity very close to the cathode can be measured [30]. In the present study, 13.5-μm-thick nickel screens with 1500 lines per inch (lpi) were mostly used. The mesh had apertures of about 10×10 $\mu\mathrm{m}^2$ with a distance of about 7 μm between apertures. As progressively thinner screens with smaller apertures were used for calibration, the pH reading asymptotically approached the actual pH value very close to the electrode. This type of calibration was performed in the manner shown by Deligianni and Romankiw [60, 61]. The real surface area of the mesh is difficult to estimate, since it is changing during plating and since it does not contribute homogeneously to the applied current density because of current distribution effects in the mesh apertures. Obviously, any ion-selective electrode such as chloride or any other available in the flat-bottomed configuration could be used simultaneously with the pH electrode to measure the concentrations of those specific ions. There are no other methods known to these authors that permit simultaneous investigation of the concentration of different ionic species in the electrode area during electrodeposition (cathodic

reaction) or dissolution (anodic reaction) within the diffusion layer at the electrode.

The electrode potential during pH measurements was monitored by a saturated mercury/mercurous sulfate (SME) reference electrode placed close to the cathode. The pH measurement cell was placed inside 1.5 L of CoFe plating solution, with the cathode at a 45° angle to the horizontal to facilitate the escape of hydrogen bubbles formed at the recessed electrode. No agitation was used, but the method can be extended to measure pH in the presence of precisely controlled agitation [60, 61]. Compared with RCH cell or paddle cell plating, the pH values observed in stagnant surface pH measurements are slightly higher owing to the lack of solution mixing, representing the worst case with respect to hydroxide formation. The reaction time of the flat-bottomed pH electrode was determined to be 4–5 s (95% pH change) for a pH change from 4 to 7 and vice versa.

Rotating-cylinder Hull (RCH) cell

During RCH cell [63] plating, deposition on cylindrical cathodes occurs with a distribution of current density along the axis. **Figure 11(a)** shows that the current distribution is induced by a cylindrical insulator placed between cathode and anode. Polished and cleaned copper cylinders (height 57 mm, diameter 15 mm) were used as working electrodes (cathode). The anode was a cylindrical cobalt sheet (>99.95% Co). Solution volume was 1 L; the change in Fe/Co ratios in the solution and the films was $\ll$1% during any experiment. Agitation was achieved by rotating the cathode at 780 rpm, a rotation speed determined to give a diffusion layer thickness equivalent to that created in a paddle cell with the paddle moving at a sinusoidally modulated speed with a frequency of one cycle per second. The current distribution along the cylinders was calibrated by electrodeposition of copper at 100% current efficiency from a solution containing 0.5 M $CuSO_4$ + 1 M H_2SO_4. For all CoFe plating experiments, it was assumed that the current distribution was the same as in **Figure 11(b)**.

Films were dc-plated at an average applied current density of −11 mA/cm^2 during 685 s at 780 rpm. The resulting film thickness was ~0.3–0.4 μm at the low-current-density end (bottom) and ~5–8 μm at the high-current-density end (top) of the cylindrical cathode. The film composition along the axis of the cylinder was measured by electron microprobe at 12 kV and 30-μm spot size using wavelength-dispersive analysis.

Electrolytes

CoFe was plated from a sulfate bath similar to the one described in Section 6 [29], using a constant Fe^{2+}/Co^{2+} ratio of 3.59. To study the effect of bath ingredients, one or several ingredients were subsequently eliminated from the above-described "fully formulated" bath. Prior to each experiment, the Fe^{3+} content of the bath was minimized by vigorous stirring in the presence of a small amount of iron powder for 20 minutes.

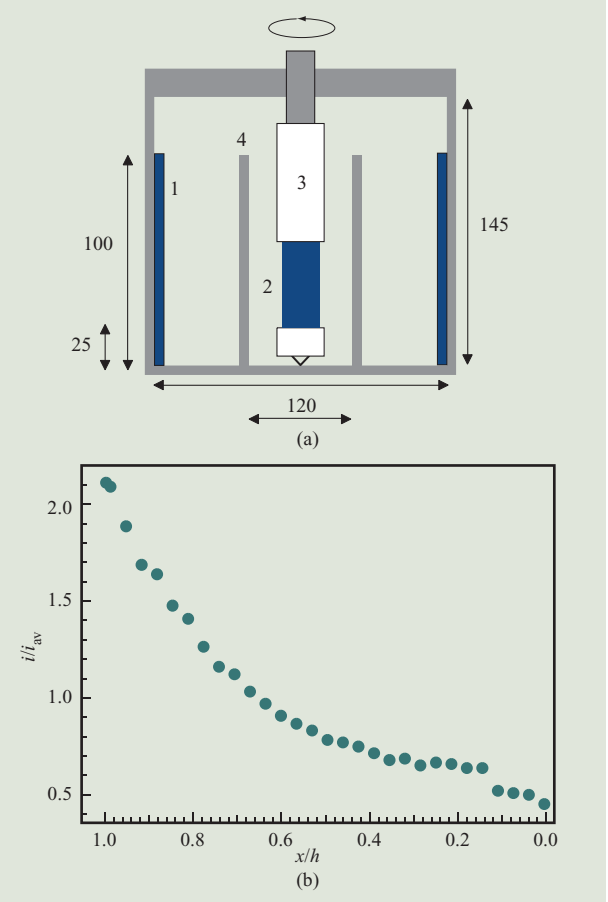

Figure 11

(a) Schematic of RCH cell: (1) Anode (cobalt); (2) working electrode (copper cylinder); (3) insulator (PTFE); (4) cylindrical insulator (polycarbonate). Dimensions are in millimeters. (b) Current distribution at the RCH cell samples under exclusion of mass-transport limitations, as calibrated using copper electrodeposition and thickness measurements. $x = 0$ corresponds to the lower end of the sample in Figure 2(a). The height h of the cylindrical samples is 57 mm. From [31], reproduced by permission of The Electrochemical Society, Inc.

Cathode pH and RCH cell: Results and discussion

Effect of SBA

As mentioned above, the incorporation of oxide or hydroxide is a major problem in electroplating of CoFe alloys. These inclusions degrade the magnetic properties, increase the stress, and darken the deposit. A sulfur-bearing additive (SBA) was found to suppress the

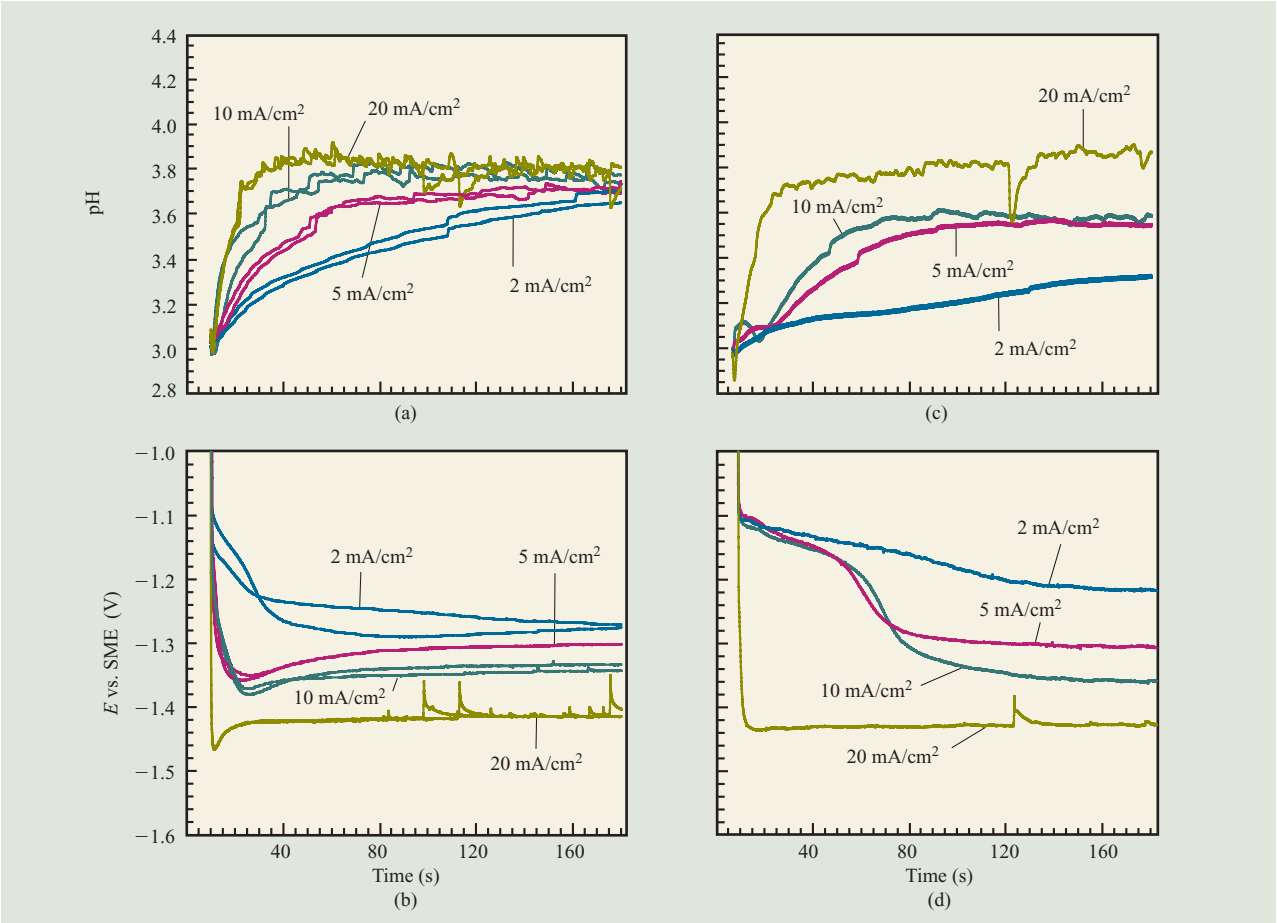

Figure 12

Surface pH (a) and potential (b) measured on the mesh cathode during galvanostatic CoFe plating from a solution containing $FeSO_4$, $CoSO_4$, H_3BO_3, and CH_3COOH at pH 3.00. The reproducibility at four different current density values is shown. Parts (c) and (d) respectively show the surface pH and potential during the same type of experiment in a bath containing a low concentration of the sulfur-bearing additive (SBA). From [31], reproduced by permission of The Electrochemical Society, Inc.

incorporation of oxides. In **Figure 12**, results of surface pH measurements in the absence of SBA and in the presence of a small concentration of SBA are shown. It can be seen that it takes tens of seconds, much longer than the response time of the pH electrode, to build up a stable pH at the surface and a total cathode potential. The higher the current density, the faster the pH reaches the steady-state value. At -2 mA/cm^2, the pH is still increasing, even after 170 s of polarization. At higher current densities, the noise becomes more important, probably due to hydrogen formation. It is interesting to note that, even at the highest current densities, the pH does not exceed 3.9. This barrier appears to be due to the buffer capacity of the acetic acid present. Also, the potential requires tens of seconds to stabilize as well. This is as expected, because the pH change can also be expressed as partial potential, which contributes to the total cathode potential.

When comparing Figures 12(b) (no SBA) and 12(d) (SBA), lower values in overpotential are consistently found during the first tens of seconds of plating in the presence of SBA and at current densities up to -10 mA/cm^2. However, toward the end of the experiment, the overpotential increases, reaching values similar to those encountered when plating without SBA. Plating at lower overpotential leads to a clearly smaller pH rise in Figure 12(c) up to -10 mA/cm^2. Apparently, fewer protons are reduced simultaneously with the metal deposition, as a result of higher current efficiency at smaller overpotentials. The observed decrease in overpotential and the drop in cathode pH are explained by the metal deposition being accelerated by SBA. If SBA inhibited proton reduction rather than accelerating

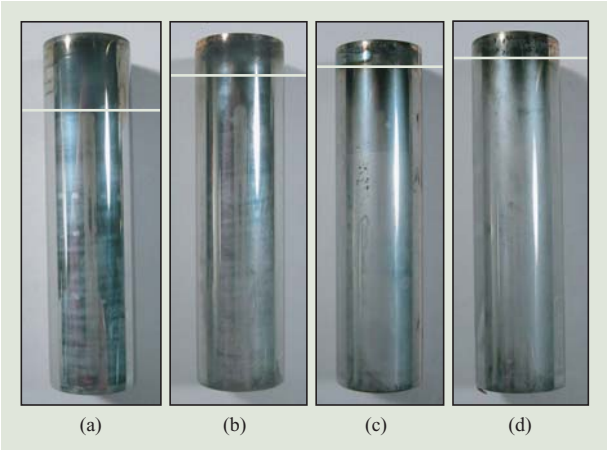

Figure 13

RCH cell samples plated in fully formulated CoFe baths containing different amounts of SBA: (a) low, (b) intermediate, (c) high, (d) very high. The bottom of the samples corresponds to the low-current-density end during plating. The average applied current density was -11 mA/cm^2, and the current distribution is shown in Figure 11. The white lines indicate the lowest point (lowest current density) where substantial dark spots occur. From [31], reproduced by permission of The Electrochemical Society, Inc.

metal deposition, the electrode overpotential would increase during the performed galvanostatic experiments. At -20 mA/cm^2, no significant difference in potential and consequently no difference in pH are observed.

Figures 12(c) and 12(d) suggest that a small amount of SBA is not sufficient to lower the pH at higher current densities. This might be due to the stagnant conditions in the cell, leading to depletion of SBA at the cathode.

Although it has only a small effect on lowering cathode pH during plating, SBA shifts the critical pH, at which the hydrolysis product α-FeO(OH) precipitates [59], to higher current density. Consequently, the occurrence of "black spots" in the films (i.e., oxide inclusions) is also moved to higher current density. **Figure 13** shows RCH cell samples plated with increasing amounts of SBA in a fully formulated CoFe bath. The first appearance of black spots, indicated by the white lines, is shifted to higher current density as the SBA concentration increases from low at the far left to high at the right. No beneficial effect is seen when the additive concentration is increased further. This indicates that the cathode pH at high current density cannot be lowered any further. In Figure 13(a), the white line corresponds to approximately -14 mA/cm^2. The occurrence of oxide inclusions is shifted to -18 mA/cm^2 in Figures 13(c) and 13(d).

A direct comparison of conditions occurring in the surface pH measurement experiments and those in the RCH cell experiments is difficult because of different

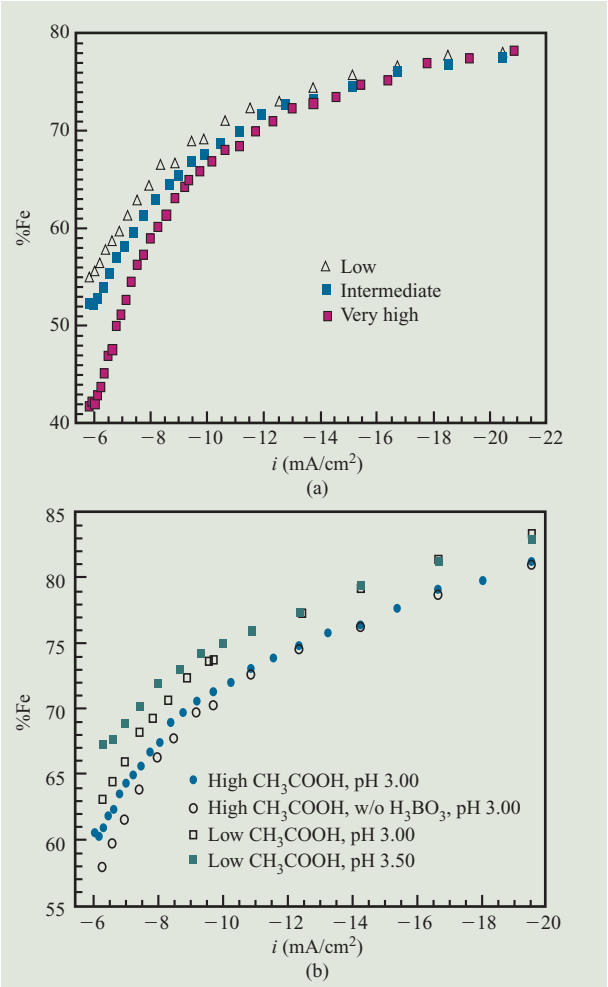

Figure 14

Composition of RCH cell samples as a function of current density, plated in a fully formulated CoFe bath (a) in the presence of different amounts of SBA; (b) with the specifications given inside the figure. From [31], reproduced by permission of The Electrochemical Society, Inc.

hydrodynamics. For a given current density, the cathode pH can be expected to be lower in the RCH cell because of the thinner diffusion layer and the faster mass transport.

In order to best observe the effects of SBA on the composition of CoFe films, RCH cell samples were plated using a high $FeSO_4/CoSO_4$ ratio in the plating bath. This generates more severe conditions which favor oxide inclusions, since the oxidation of Fe^{2+} to Fe^{3+} and the precipitation of ferric hydroxides are intensified with higher Fe^{2+} concentration. **Figure 14(a)** shows that a higher SBA concentration lowers the iron content, especially at low current density, where it significantly opposes a rise in pH. At current densities beyond

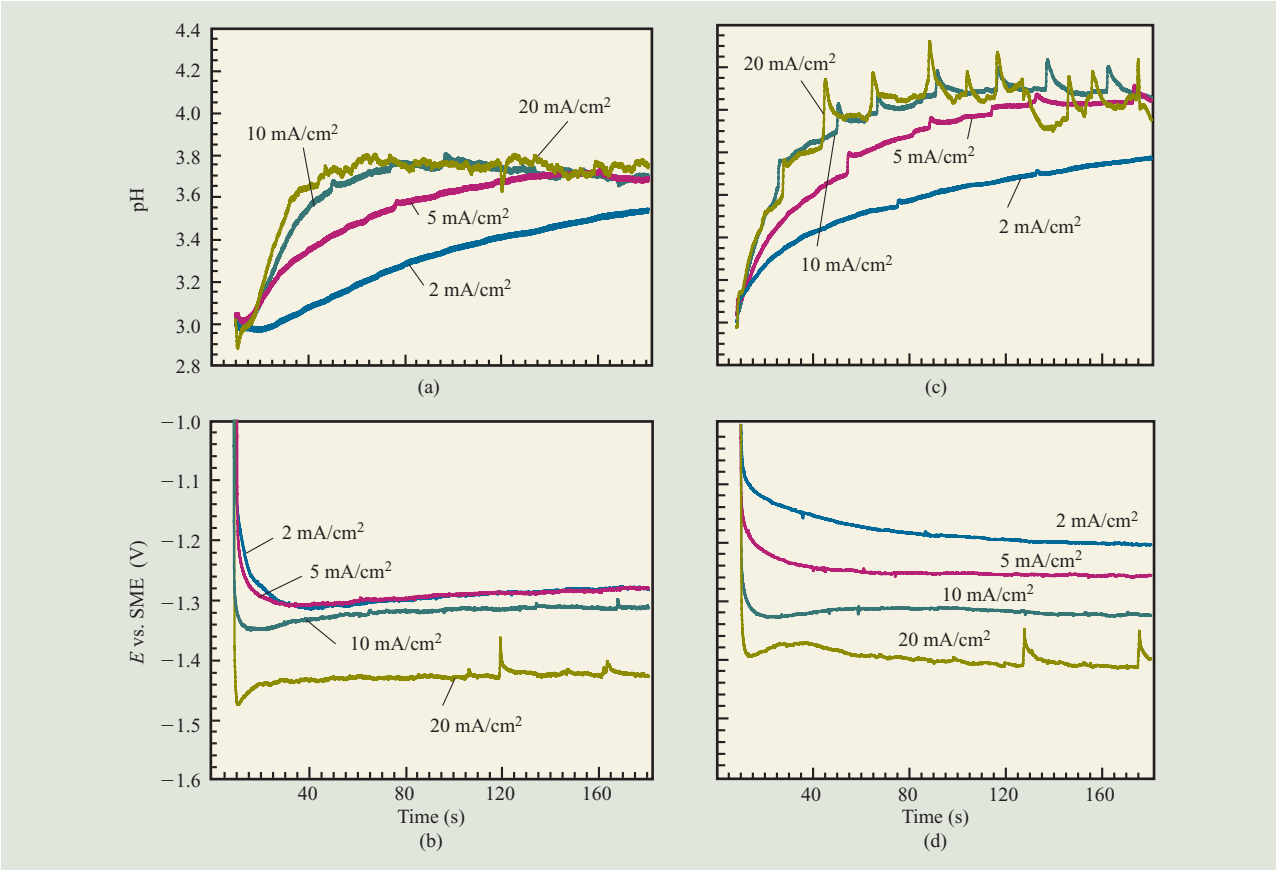

Figure 15

Surface pH (a) and potential (b) as a function of time and current density during plating in a bath containing $FeSO_4$, $CoSO_4$, and CH_3COOH (no H_3BO_3). Parts (c) and (d) show the same experiments in a bath containing $FeSO_4$, $CoSO_4$, H_3BO_3, CH_3COOH, and a fluorosurfactant. From [31], reproduced by permission of The Electrochemical Society, Inc.

-18 mA/cm^2, no effect of SBA concentration on composition is observed, because the pH rise can no longer be suppressed, as in Figure 12(c). This is in agreement with the identical appearance of black spots at around -18 mA/cm^2 at high SBA concentrations in Figures 13(c) and 13(d).

Effects of acetic acid (HAc), boric acid, and surfactant

A series of time-dependent pH and potential measurements were performed using the same bath composition as in Figures 12(a) and 12(b) (not containing SBA), except that acetic acid (HAc) was eliminated. The current density ranged from -2 to -50 mA/cm^2. In contrast to Figure 12, where the pH does not exceed 3.9, here the pH rises to around 6.5. Without HAc, the buffer capacity is mainly determined by boric acid, which has a pK_a of about 6.8 when concentrated [64]. As discussed above, such a high pH inevitably leads to oxide inclusions. By contrast, the overpotential is not significantly influenced by the presence of HAc, implying that HAc is not actively involved in the plating mechanism.

Figure 14(b) shows the change in thin-film composition when plating in a fully formulated bath containing two different concentrations of HAc. The RCH cell sample plated in the lower concentration of HAc had higher iron content over the whole range of current densities because of the slightly higher pH reached at each point of the sample due to the lower buffer capacity of the bath. As a result, oxide inclusions were already observed at about -13.5 mA/cm^2. The effect of bulk pH on composition is also shown in Figure 14(b). When the bulk pH was increased from 3.00 to 3.50, an increase in iron content was observed only at the low-current-density end of the electrode. This happens because at low current density the cathode pH has not yet reached the buffering limit of HAc and is still a function of the bulk pH. At high current density, however, the cathode pH is solely governed by the buffer capacity of HAc.

The role of boric acid in electroplating baths as a brightener, buffer, or stress reliever is still not well understood, despite extensive literature on this subject [64–66]. Boric acid has a long tradition in electroplating technology, e.g., in NiFe plating baths [3]. The present study examined the effect of boric acid on cathode pH and composition in CoFe plating. The results are quite surprising. While one would hardly expect boric acid to act as an effective acidic buffer at pH 3–4, a comparison of **Figure 15(a)** and Figure 12(a) shows that the pH values reached *with* boric acid are generally slightly *higher*, i.e., even more basic, than in its absence. The difference is most significant at very low current density, such as -2 mA/cm^2. Even at -20 mA/cm^2, the pH does not exceed 3.8 in the absence of boric acid. The potentials in **Figure 15(b)** differ little from those measured in Figure 12(b). The slightly higher cathode pH in the presence of boric acid, consistently observed in CoFe deposition experiments, may not necessarily be beneficial in the plating of CoFe alloys except when a higher iron content in the films is desired. The function of boric acid is hard to explain without further experiments, especially considering the NiFe plating literature, in which generally increasing boric acid concentration is reported to cause a decrease of the limiting current for proton reduction [66].

Consistent with the measured lower pH without boric acid, the compositional analysis in Figure 14(b) reveals slightly less iron in the film, especially at low current densities, where the pH effect is most pronounced. This demonstrates again the very sensitive and close dependence of the composition, and thus the mechanism, on the cathode surface pH.

The results with the perfluorinated surfactant, shown in **Figures 15(c)** and **15(d)**, are unexpected as well. This surface-active species is present only at a very low concentration, and is presumably quite inert chemically (complexation or chemisorption should be weak because of high charge delocalization in the anion head). Nevertheless, up to -20 mA/cm^2, the overpotential in Figure 15(d) is clearly smaller than that in Figure 12(b). On the other hand, the cathode pH in the presence of surfactant [Figure 15(c)] is significantly higher than in its absence [Figure 12(a)], 4.1 vs. 3.8 at -20 mA/cm^2 after 170 s. Such differences are important when taking into consideration that the solubility of α-FeO(OH) decreases by a factor of approximately 100 between pH 3 and pH 4 [59]. The decrease in overpotential and rise in pH can only be explained by the surfactant facilitating the evolution of hydrogen, leading to a higher partial current density for proton reduction. Since the surfactant lowers the surface tension, hydrogen bubbles are released from the surface more readily, which increases the mass transport in the diffusion layer and hence accelerates hydrogen evolution.

Surface pH behavior in the fully formulated CoFe plating bath

A clear pH barrier of 4.4 was observed when HAc and SBA were present together. This barrier was not exceeded even at -50 mA/cm^2 because of the buffering action of HAc ($pK_a = 4.75$). In a fully formulated bath, the behavior is determined by a current-density-dependent competition between the SBA and the surfactant. The SBA present partially lowers the overpotential at low current density, up to -5 mA/cm^2. In this current density range, the pH is very similar to that of Figure 12(c), where the SBA governs the behavior. This is also demonstrated in **Figure 16(a)**, which shows the cathode pH reached in different baths during plating at -2 mA/cm^2. At higher current density, the fluorosurfactant determines the pH behavior and increases the surface pH considerably. Thus, the fully formulated bath with all additives exceeds the pH reached in a no-additive bath containing a low concentration of SBA. This is due primarily to the presence of surfactant, as demonstrated in **Figure 16(b)** for -10 mA/cm^2.

Clearly, additives are needed for dealing with a wide range of issues such as wetting, stress, and current efficiency. However, in order to understand their overall effects and the complex interplay between different additives, their impact on surface pH and oxide inclusions has to be considered. At the most basic level, a consistent correlation between surface pH and composition was observed, the CoFe film being richer in iron with increasing pH. On the basis of the findings of this study, a simple qualitative model for the deposition mechanism, involving pH-dependent adsorption of ferric hydroxides, was proposed [31].

This study demonstrated the usefulness of combined *in situ* surface pH and RCH cell experiments in optimizing the deposition of alloys that react sensitively to surface pH changes. These techniques allow for efficient testing of plating baths and plating conditions, while giving valuable information necessary for a profound understanding of the plating mechanism.

8. Domain control in high-moment materials

For high-data-rate write head designs, the control of the magnetic domain structure in the yoke is critical. To achieve fast flux reversal and good high-frequency efficiency, an orientation of the net magnetization perpendicular to the flux propagation path is desirable. The micromagnetic structure of the write head can be strongly affected by mechanical stresses if the magnetic material exhibits high magnetostriction. This is the case for most of the high-moment materials, i.e. high-iron NiFe, CoFe (except for ~90/10 compositions), and high-iron CoNiFe. A combination of high magnetostriction and high as-plated internal stress can be particularly

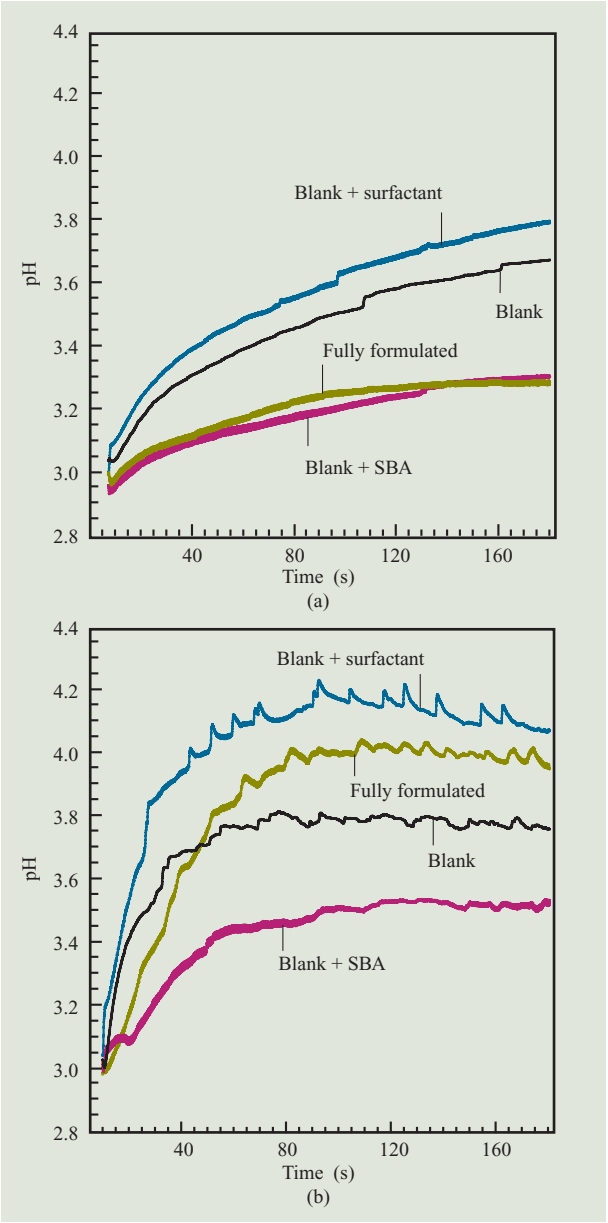

Figure 16

Surface pH measured on a mesh cathode during plating in different electrolytes at (a) -2 mA/cm^2 and (b) -10 mA/cm^2. The "blank" solution contained $FeSO_4$, $CoSO_4$, H_3BO_3, and CH_3COOH. From [31], reproduced by permission of The Electrochemical Society, Inc.

undesirable. This is also true for the write pole, where magneto-elastic coupling with tensile stress at the air-bearing surface (ABS) creates a strong induced perpendicular anisotropy, which affects the flux dynamics in the pole and can potentially create remanence effects.

Among the alloys with saturation flux density at or above 2.0 T, all have substantial magnetostriction and as-plated internal stress. In order to obtain the correct domain orientation in these materials, it becomes necessary to compensate for the problem by a careful annealing regime (to decrease or properly manage stress) and by modifications in design (to reduce shape-induced anisotropy, etc.).

The only high-moment material in which zero or very low ($\pm$1–3 ppm) values of magnetostriction can be easily obtained is CoFeCu ($Co_{90}Fe_{10}$ has a narrower range of low magnetostriction and has higher internal stress). For head yokes plated with CoFeCu, it has been shown [22, 67] by Kerr imaging that the correct domain orientation—mostly edge closure domains—is obtained even without the need for post-plating anneal; this is in contrast to similar heads plated with $Ni_{45}Fe_{55}$, which show a more complicated pattern that includes undesirable axial domains. The difference is accentuated by further processing steps that tend to increase stress, such as the deposition of an overcoat layer and the lapping of the head to the proper throat height.

For the high-magnetostriction high-moment materials, and especially for high-iron CoFe, the desired domain orientation—easy-axis transversal to the long axis of the plated feature—is more difficult to obtain. To prove feasibility, stripes of magnetic material ($Co_{36.2}Fe_{63.8}$ and $Ni_{45}Fe_{55}$) were plated either on flat substrates between parallel stripes of resist or on top of stripes of resist oriented in a perpendicular direction ("on topography"), as shown in **Figure 17**. The width of the magnetic stripes (20 μm) was similar to the yoke width of production-type head designs. The resulting samples were subjected to two thermal treatment steps of varying length: a "hard-bake" step at 180°C, which is part of the resist-curing process and causes the resist to shrink while inducing stress in the adjacent magnetic stripes; and an annealing step at 240°C in a magnetic field of 12 kG perpendicular to the direction of the magnetic stripes [68]. Kerr imaging revealed (Figures 4 and 5 in [68]) that the remanent magnetization of as-plated stripes was along the stripes, in contrast to the magnetization of unpatterned areas, which was parallel to the annealing field. Domain orientation after the thermal treatment depends on its parameters, especially in the case of resist stripes perpendicular to the magnetic stripes. It was found (see Figure 17 and **Figure 18**) that the preferred way to rotate the magnetic domains to a direction perpendicular to the stripes is to cure the resist incompletely in a short hard-bake step (e.g., 1 h), so that substantial shrinkage still occurs during the second, magnetic-field annealing step. After annealing, the shrunken resist gives rise to a compressive force in the direction of the long axis of the stripe, consequently resulting in stress-induced anisotropy perpendicular to the stripe for a magnetic material with positive magnetostriction constant. The increase in stress-induced

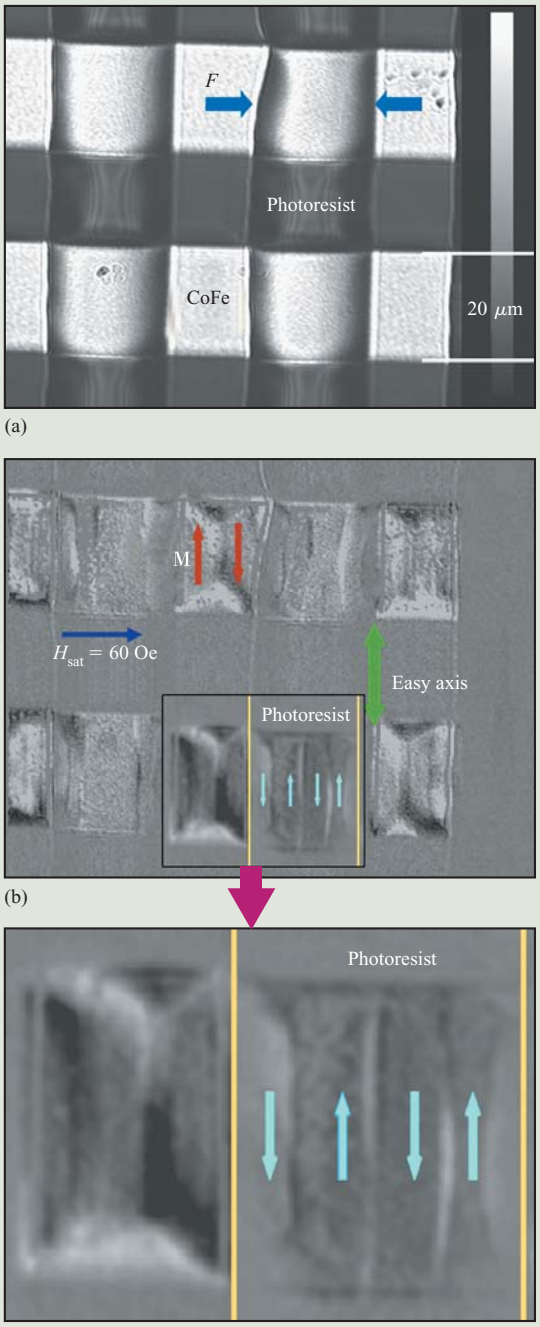

Figure 17

(a) Plated CoFe stripes on resist topography after final anneal. Resist hard-bake 1 hour @ 180°C. *F* indicates the force acting on the magnetic material due to resist shrinkage. (b) Longitudinal Kerr image of the remanent state of 20-μm-wide CoFe stripes on topography after application of a horizontal field of 60 Oe. Hard-bake: 1 hour; anneal: 2 hours. The Kerr sensitivity is horizontal. (c) Enlarged Kerr image of the boxed area. From [68], reproduced by permission of The Electrochemical Society, Inc.

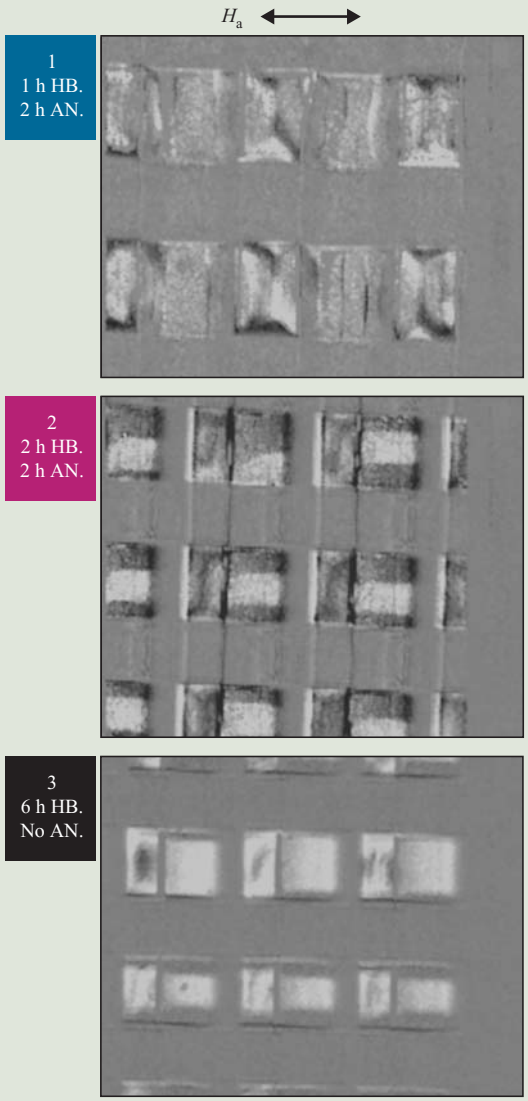

Figure 18

Longitudinal Kerr image of the remanent state of 20-μm-wide CoFe stripes on topography after application of a horizontal field H_a of 60 Oe. Hard-bake (HB) and anneal (AN) conditions: as in Figure 17. The Kerr sensitivity is horizontal. Note that for Cases 2 and 3 (6 or 2 hr hard-bake) the magnetization is still aligned horizontally, parallel to the long axis of the stripes. In contrast, for Case 1 (1 hr hard-bake) the anneal causes formation of vertical domains. From [68], reproduced by permission of The Electrochemical Society, Inc.

anisotropy is reflected in a decreased squareness of the easy-axis *B*–*H* loops, as shown in **Figure 19**. The deposition of an alumina overcoat causes additional stress which must be taken into account when optimizing the process parameters.

In summary, even for a material with a very high magnetostriction (60×10^{-6} for $Co_{36.2}Fe_{63.8}$), a narrow

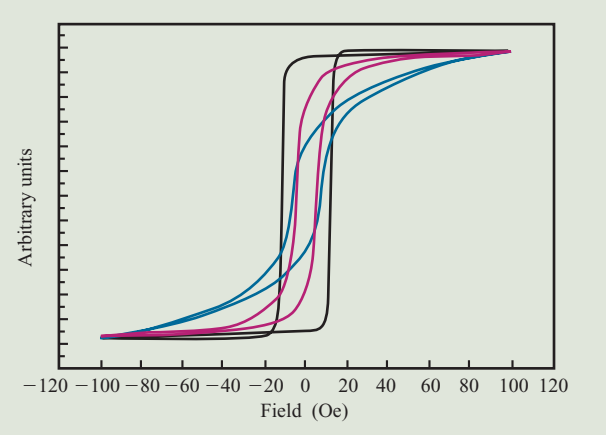

Figure 19

Hysteresis loops along the CoFe stripes plated on topography, for 2-hour anneal, 1-hour hard-bake (blue curves); 2-hour anneal, 2-hour hard-bake (red curves); and no anneal, 6-hour hard-bake (black curves).

but (for practical applications) sufficient window of hard-bake/anneal conditions exists to achieve the preferred domain configuration.

Concluding remarks

The last decade has seen rapid progress in the electrodeposition of soft magnetic alloys with ever higher moment, from 1.0 T for permalloy to 1.7 T ($Ni_{45}Fe_{55}$), 1.8–2.0 T (CoFeCu), 2.0–2.2 T (CoNiFe), 2.0–2.2 T (high-iron NiFe), and finally to 2.4–2.5 T (CoFe). With this last step, the promise held by the Co–Ni–Fe ternary composition diagram seems to have been exhausted, since the compositions corresponding to the highest-moment stable alloys in this system have been plated successfully. Since there are no other soft magnetic elements that can be codeposited with Co, Ni, and/or Fe, it would appear that we are at the end of this particular road, and any future improvements in magnetic recording heads will come from elsewhere. Fortunately, antiferromagnetically coupled (AFC) media [12], introduced in 2001, allowed the areal density to increase further with no need to increase the medium coercivity. Nevertheless, the areal density is quickly reaching the limit at which longitudinal recording (high bit area/bit volume ratio) will have to be replaced by perpendicular recording (low bit area/bit volume ratio) [69]. This drastic change of technology should make it possible to push the superparamagnetic limit beyond one terabit per square inch. Since the performance of perpendicular bits will also eventually benefit from higher magnetic moment, it is worth reconsidering whether there are any remaining ways to boost the saturation flux density.

First, an experimental comment. Since future magnetic moment increases, if any, are likely to be smaller than in the recent past, the test vehicles, electrical contacts, and measurement techniques will have to be designed very carefully so as to achieve high accuracy and reproducibility. In particular, variations in thickness and composition across the samples have to be minimized, and areas near contacts should be discarded.

Once techniques are available for reliably measuring small changes in moment, there are at least three simple ideas to follow. One is to push alloy purity to the limit, eliminating to the extent possible extraneous elements (O, C, N, S) and also voids and intergranular space so as to generate a deposit of maximum density. Another is to pursue alloys in which a small amount of a high-spin-transition metal M, ferromagnetically coupled to the main components, enhances the magnetic moment of $Co_xFe_yM_{1-x-y}$ relative to Co_xFe_{1-y}. Such a case was described by Chen [70] for additions of manganese. Since electroplating at practical rates generates alloys in a non-equilibrium state, published results obtained with slowly cooled bulk samples can serve only for general guidance. A third direction worth exploring is to learn more about the effects of the degree of ordering and the best ways to use thermal annealing in order to maximize magnetic moment. These approaches offer additional possible advantages, in areas such as reduction of coercivity, increase of electrical resistance, or improvements in corrosion resistance.

Beyond such potential small improvements, one can try to boldly go into deeply metastable territory and pursue fcc-phase high-iron alloys. The fcc phase of iron is highly unstable in bulk at ambient temperatures, but it is very attractive in principle, since theoretical calculations have shown it to be capable of reaching magnetic moments of >2.5 T [71], provided that the lattice parameter is in the right range. Experimentally, fcc iron can be stabilized in thin-film form by epitaxial growth upon [72, 73], and/or by sandwiching between [74], layers of stable fcc metals such as copper or palladium. When so generated, fcc iron can have an extremely high saturation flux density, as high as 3.4 T (up to ~50% higher than the value for bulk bcc iron) according to one report [74]. Unfortunately, the thickness of the stable fcc metal required for stabilization of fcc iron is larger than the thickness of the iron film itself; the result is an overall unremarkable magnetic moment. It is conceivable, however, that some high-iron alloys are less unstable in the fcc state and can be stabilized by much thinner films of a stable fcc metal (or metal alloy), to yield multilayered films with a global magnetic moment exceeding 2.5 T. Careful lattice parameter matching between substrate and deposit may be needed, since the magnetic moment of fcc iron and its alloys has been calculated to be extremely dependent on

the lattice parameter [71, 75, 76]. The electroplating technique can assist in generating such films, since electrodeposition can be performed under highly irreversible conditions and as a result can form the phase that is easiest to nucleate—in this case, fortuitously, the same phase as the fcc substrate due to epitaxial seeding—rather than the thermodynamically stable phase. In this way, electrodeposition at high current density resembles thermal quenching of a liquid. However, any thermal excursions of such "thermodynamically challenged" films will have to be managed carefully, since at high temperatures the unstable fcc phase is likely to revert to bcc structure.

Acknowledgments

We wish to thank our many colleagues who took part in the work on which this review paper is based: A. Baer, E. Brinkman, F. Cardone, J. Cotte, V. Deline, T. E. Dinan, M. Flotta, E. Grochowski, T. Harris, A. Hixson-Goldsmith, S. Krongelb, A. Kumar, M. Last, J. G. McCord, A. Medina, D. Miller, V. Nikitin, M. Toney, E. P. Velasco, and S. Yuan.

References

1. J. C. Mallinson, *The Foundations of Magnetic Recording*, Academic Press, Inc., New York, 1987.
2. S. X. Wang and A. M. Taratorin, *Magnetic Information Storage Technology*, Academic Press, Inc., New York, 1999.
3. P. C. Andricacos and L. T. Romankiw, "Magnetically Soft Materials in Data Storage: Their Properties and Electrochemistry," *Advances in Electrochemical Science and Engineering*, Vol. 3, Heinz Gerischer and Charles Tobias, Eds., VCH, New York, 1994, pp. 227–321.
4. L. T. Romankiw and D. A. Thompson, "Thin Film Inductive Transducer," U.S. Patent 4,295,173, October 13, 1981.
5. L. T. Romankiw, "Thin Film Inductive Heads: From One to Thirty One Turns," *Magnetic Materials, Processes and Devices*, L. T. Romankiw and D. A. Herman, Jr., Eds., **PV 90-8**, The Electrochemical Society Proceedings Series, Princeton, NJ, 1990, p. 39.
6. L. T. Romankiw, "Thirty Years of Thin Film Magnetic Heads for the Hard Disc Drives—The Challenges and Solutions of Problems 30 Years Ago and Today," *J. Magn. Soc. Jpn.* **24**, No. 1, 1–4 (2000).
7. D. A. Thompson, "Magnetoresistive Transducers in Magnetic Recording," *Proceedings of the 1974 AIP Conference on Magnetism and Magnetic Materials*, No. 24, 1975, pp. 528–533.
8. L. T. Romankiw, "Integrated Magnetoresistive Read, Inductive Write, Batch Fabricated Magnetic Head," U.S. Patent 3,908,194, September 23, 1975.
9. C. H. Bajorek, S. Krongelb, L. T. Romankiw, and D. A. Thompson, "An Integrated Magnetoresistive Read, Inductive High Density Recording Head." *Proceedings of the 1974 AIP Conference on Magnetism and Magnetic Materials*, No. 24, 1975, p. 548.
10. C. Tsang, R. E. Fontana, T. Lin, D. E. Heim, V. S. Speriosu, B. A. Gurney, and M. L. Williams, "Design, Fabrication and Testing of Spin Valve Read Heads for High Density Recording," *IEEE Trans. Magn.* **30**, No. 6, 3801–3806 (1994).
11. C. Tsang, T. Lin, S. MacDonald, M. Pinarbasi, N. Robertson, H. Santini, M. Doerner, T. Reith, V. Lang, T. Diola, and P. Arnett, "5 Gbits/in^2 Recording Demonstration with Conventional AMR Dual Element Heads and Thin Film Disks," *IEEE Trans. Magn.* **33**, No. 5, 2866–2871 (1997).
12. E. E. Fullerton, D. T. Margulies, M. E. Schabes, M. Carey, B. A. Gurney, A. Moser, M. Best, G. Zeltzer, K. Rubin, H. Rosen, and M. Doerner, "Antiferromagnetically Coupled Magnetic Media Layers for Thermally Stable High-Density Recording," *Appl. Phys. Lett.* **77**, No. 23, 3806–3808 (2000).
13. E. E. Castellani, J. V. Powers, and L. T. Romankiw, "Nickel–Iron (80–20) Alloy Thin Film Electroplating Method and Electrochemical Treatment and Plating Apparatus," U.S. Patent 4,102,756, July 25, 1978.
14. N. C. Anderson and C. R. Grover, Jr., "Electroplating of Ni–Fe Alloy for Uniformity of Ni/Fe Ratio Using a Low Density Plating Current," U.S. Patent 4,279,707, July 21, 1981.
15. J. V. Powers and L. T. Romankiw, "Electroplating Cell Including Means to Agitate the Electrolyte in Laminar Flow," U.S. Patent 3,652,442, March 28, 1972.
16. L. T. Romankiw, "Elimination of Undercut in an Anodically Active Metal During Chemical Etching," U.S. Patent 3,853,715, December 10, 1974.
17. L. T. Romankiw, "Use of AZ-Type Photoresist as Insulation in Multiturn Thin Film Recording Heads," *IBM Tech. Disclosure Bull.* **23**, No. 6, 2584–2585 (1980).
18. E. E. Castellani, I. M. Croll, A. T. Pfeiffer, and L. T. Romankiw, "Fine Line Circuit Fabrication and Photoresist Application Therefor," U.S. Patent 4,315,985, February 16, 1982.
19. R. L. Anderson, E. E. Castellani, P. M. McCaffrey, and L. T. Romankiw, "Method for Treating Magnetic Alloys to Increase the Magnetic Permeability," U.S. Patent 4,003,768, January 18, 1977.
20. N. Robertson, H. L. Hu, and C. Tsang, "High Performance Write Head Using NiFe 45/55," *IEEE Trans. Magn.* **33**, No. 5, Part 1, 2818–2820 (1997).
21. J.-W. Chang, P. C. Andricacos, B. Petek, P. L. Trouilloud, and L. T. Romankiw, "Electrodeposited High $4\pi M_s$ CoFeCu for Thin Film Recording Heads," *Magnetic Materials, Processes and Devices V*, L. T. Romankiw, S. Krongelb, and C. H. Ahn, Eds., **PV 98-20**, The Electrochemical Society Proceedings Series, Pennington, NJ, 1999, pp. 488–508.
22. E. I. Cooper, Y. Hsu, L. T. Romankiw, J. G. McCord, and V. Nikitin, "Electroplated CoFeCu Films in Write Heads: Plating and Magnetic Evaluation," *Magnetic Materials, Processes and Devices VI*, S. Krongelb, L. T. Romankiw, J.-W. Chang, W. Schwartzacher, and C. H. Ahn, Eds., **PV 2000-29**, The Electrochemical Society Proceedings Series, Pennington, NJ, 2001, pp. 264–275.
23. P. Trouilloud, L. T. Romankiw, J.-W. Chang, and K. C. Lin, "Magnetic Properties of Copper Laminated Magnetic CoFeCu Films Deposited from a Single Plating Bath by Current Modulation," *Magnetic Materials, Processes and Devices VI*, S. Krongelb, L. T. Romankiw, J.-W. Chang, W. Schwartzacher, and C. H. Ahn, Eds., **PV 2000-29**, The Electrochemical Society Proceedings Series, Pennington, NJ, 2001, pp. 276–286.
24. M. Ramasubramanian, J. Lam, A. Hixson-Goldsmith, A. Medina, T. Dinan, N. Robertson, T. Harris, and S. Yuan, "Electrodeposition and Performance Evaluation of High Moment Nickel–Iron Films," *Magnetic Materials, Processes and Devices VII and Electrodeposition of Alloys*, S. Krongelb, L. T. Romankiw, J.-W. Chang, Y. Kitamoto, J. W. Judy, C. Bonhôte, G. Zangari, and W. Schwarzacher, Eds., **PV 2002-27**, The Electrochemical Society Proceedings Series, Pennington, NJ, 2003, pp. 298–306.
25. T. Osaka, M. Takai, K. Hayashi, Y. Sogawa, K. Ohashi, Y. Yasue, M. Saito, and K. Yamada, "New Soft Magnetic CoFeNi Plated Films with High B_s = 2.0–2.1 T," *IEEE Trans. Magn.* **34**, 1432–1434 (1998).
26. I. Tabakovic, S. Reimer, P. Jallen, V. Inturi, and A. Thayer, "Effect of Additives in the Electrochemical Preparation of Soft Magnetic CoNiFe Films," *Magnetic Materials, Processes and Devices V*, **PV 1998-20**, L. T. Romankiw, S. Krongelb, and C. H. Ahn, Eds., The Electrochemical Society Proceedings Series, Pennington, NJ, 1999, pp. 531–544.

27. C. Bonhôte, M. Ramasubramanian, E. P. Velasco, E. I. Cooper, and L. T. Romankiw, "High Moment Electrodeposited CoNiFe," *Magnetic Materials, Processes and Devices VII and Electrodeposition of Alloys*, S. Krongelb, L. T. Romankiw, J.-W. Chang, Y. Kitamoto, J. W. Judy, C. Bonhôte, G. Zangari, and W. Schwarzacher, Eds., **PV 2002-27**, The Electrochemical Society Proceedings Series, Pennington, NJ, 2003, pp. 254–261.
28. R. Bozorth, *Ferromagnetism*, Van Nostrand, Princeton, NJ, 1951.
29. C. Bonhôte, H. Xu, E. I. Cooper, and L. T. Romankiw, "Electroplated 2.4 Tesla CoFe Films," *Magnetic Materials, Processes and Devices VII and Electrodeposition of Alloys*, S. Krongelb, L. T. Romankiw, J.-W. Chang, Y. Kitamoto, J. W. Judy, C. Bonhôte, G. Zangari, and W. Schwarzacher, Eds., **PV 2002-27**, The Electrochemical Society Proceedings Series, Pennington, NJ, 2003, pp. 319–327.
30. L. T. Romankiw, "pH Changes at the Cathode During Electrolysis of Ni, Fe, Cu and Their Alloys and Simple Technique for Measuring pH Changes at Electrodes," *Electrodeposition Technology, Theory and Practice*, L. T. Romankiw and D. R. Turner, Eds., **PV 87-17**, The Electrochemical Society Proceedings Series, Pennington, NJ, 1987, pp. 301–325.
31. P. Kern, C. Bonhote, and L. T. Romankiw, "In-Situ Surface pH Measurements and Rotating Cylinder Hull Cell—A Powerful Combination of Methods for Investigation of Iron Group Metal Alloy Plating," *Magnetic Materials, Processes and Devices VII and Electrodeposition of Alloys*, S. Krongelb, L. T. Romankiw, J.-W. Chang, Y. Kitamoto, J. W. Judy, C. Bonhôte, G. Zangari, and W. Schwarzacher, Eds., **PV 2002-27**, The Electrochemical Society Proceedings Series, Pennington, NJ, 2003, pp. 328–350.
32. J.-W. Chang, P. C. Andricacos, B. Petek, and L. T. Romankiw, "Electrodeposition of High M_s CoFeCu Alloys for Recording Heads," *Magnetic Materials, Processes and Devices/1991*, L. T. Romankiw and D. A. Herman, Jr., Eds., **PV 92-10**, The Electrochemical Society Proceedings Series, Pennington, NJ, 1992, pp. 275–287.
33. J.-W. Chang and L. T. Romankiw, "Electrodeposited Superlattices of CoFe/Cu and NiFe/Cu," *Magnetic Materials, Processes and Devices/1993*, L. T. Romankiw and D. A. Herman, Jr., Eds., **PV 94-6**, The Electrochemical Society Proceedings Series, Pennington, NJ, 1994, pp. 223–232.
34. P. C. Andricacos and N. Robertson, "Future Directions in Electroplated Materials for Thin Film Recording Heads," *IBM J. Res. & Dev.* **42**, No. 5, 671–680 (1998).
35. C. G. Ye, Y. W. Kim, and S. Y. Kim, "Composition and Magnetic Properties of CoFeCu Alloys According to Electrolysis Conditions," *Han'guk Pyomyon Konghak Hoechi* **30**, No. 1, 3–12 (1997).
36. E. M. Kakuno, N. Mattoso, W. H. Schreiner, D. H. Mosca, and M. P. Cantao, "Structure, Composition, and Morphology of Electrodeposited $Co_{0.9}Fe_{0.1}$(Cu) Alloys," *J. Electrochem. Soc.* **144**, No. 10, 3624–3628 (1997).
37. J. Y. Park and M. G. Allen, "Development of Magnetic Materials and Process Techniques Applicable to Integrated Micromagnetic Devices," *J. Micromech. & Microeng.* **8**, No. 4, 307–316 (1998).
38. G. Poupon, "Optimization of CoFeCu Alloy for Magnetic Components," *Magnetic Materials, Processes and Devices V*, L. T. Romankiw, S. Krongelb, and C. H. Ahn, Eds., **PV 98-20**, The Electrochemical Society Proceedings Series, Pennington, NJ, 1999, pp. 509–518.
39. M. P. Gigandet, F. X. Perrin, J. Pagetti, and G. Poupon, "The Influence of Cu Content on the Corrosion Resistance of Co–Fe–Cu Magnetic Alloys in Aqueous Environments," *Mater. Corros.* **51**, No. 6, 418–423 (2000).
40. G. F. Smith and W. H. McCurdy, Jr., "2,9-Dimethyl-1,10-Phenanthroline. New Specific in Spectrophotometric Determination of Copper," *Anal. Chem.* **24**, 371 (1952).
41. T. Osaka, "Electrodeposition of Highly Functional Thin Films for Magnetic Recording Devices of the Next Century," *Electrochim. Acta* **45**, 3311–3321 (2000).
42. I. Tabakovic, S. Riemer, R. Kvitek, P. Jallen, and V. Inturi, "Origin of Inclusion of Foreign Elements During the Electrodeposition of Soft Magnetic NiFe, CoNiFe and CoNiFeO Alloys: SIMS and XPS Analysis," *Magnetic Materials, Processes and Devices VI*, S. Krongelb, L. T. Romankiw, J.-W. Chang, W. Schwartzacher, and C. H. Ahn, Eds., **PV 2000-29**, The Electrochemical Society Proceedings Series, Pennington, NJ, 2001, pp. 253–263.
43. K. Ohashi, Y. Yasue, M. Saito, K. Yamada, T. Osaka, M. Takai, and K. Hayashi, "Newly Developed Inductive Write Head with Electroplated CoNiFe Film," *IEEE Trans. Magn.* **34**, 1462–1464 (1998).
44. T. Osaka, M. Takai, K. Hayashi, K. Ohashi, M. Saito, and K. Yamada, "A Soft Magnetic CoNiFe Film with High Saturation Magnetic Flux Density and Low Coercivity," *Nature* **392**, No. 6678, 796–798 (1998).
45. T. Osaka, M. Takai, K. Hayashi, Y. Sogawa, K. Ohashi, Y. Yasue, M. Saito, and K. Yamada, "New Soft Magnetic CoNiFe Plated Films with High B_s = 2.0–2.1 T," *IEEE Trans. Magn.* **34**, No. 4, 1432–1434 (1998).
46. C. Bonhôte, J. Lam, and M. Last, "Properties of DC Plated 2.4 Tesla CoFe Alloys," to be published in *Magnetic Materials, Processes and Devices VIII*, The Electrochemical Society Proceedings Series, Pennington, NJ, 2005.
47. N. Mattoso, V. Fernandes, M. Abbate, W. H. Schreiner, and D. H. Mosca, "Structural and Chemical Characterization of Fe–Co Alloys Prepared by Electrodeposition," *Electrochem. Solid State Lett.* **4**, No. 4, C20–C22 (2001).
48. N. V. Myung and K. Nobe, "Electrodeposited Iron Group Thin-Film Alloys Structure–Property Relationship," *J. Electrochem. Soc.* **148**, No. 3, C136–C144 (2001).
49. L. Ricq, F. Lallemand, M. Gigandet, and J. Pagetti, "Influence of Sodium Saccharin on the Electrodeposition and Characterization of CoFe Magnetic Film," *Surf. Coat. Technol.* **138**, No. 2–3, 278–283 (2001).
50. E. M. Kakuno, D. H. Mosca, I. Mazzaro, N. Mattoso, W. H. Schreiner, M. A. B. Gomes, and M. P. Cantao, "Structure, Composition, and Morphology of Electrodeposited Co_xFe_{1-x} Alloys," *J. Electrochem. Soc.* **144**, No. 9, 3222–3226 (1997).
51. K. Y. Sasaki and J. B. Talbot, "Electrodeposition of Iron-Group Metals and Binary Alloys from Sulfate Baths," *J. Electrochem. Soc.* **145**, No. 3, 981–990 (1998).
52. N. Mitsumoto, S. Ichioka, and S. Takeuchi, "Method of Plating an Iron–Cobalt Alloy on a Substrate," U.S. Patent 4,208,254, June 17, 1980.
53. S. S. Abd El Rehim, K. Khaled, A. M. S. Abulkibash, and M. Emad, "Electroplating of CoFe Alloys from Aqueous Acetate Baths," *Trans. Inst. Met. Finish.* **78**, No. 1, 41–43 (2000).
54. X. Liu, P. Evans, and G. Zangari, "Electrodeposited Co–Fe Based Alloys Films for High Moment Magnetic Recording Write Heads," *Electrochemical Technology Applications in Electronics*, **PV 99-34**, The Electrochemical Society Proceedings Series, Pennington, NJ, 2000, pp. 255–262.
55. I. Shao, P. M. Vereecken, C. L. Chien, R. C. Cammarata, and P. C. Searson, "Electrochemical Deposition of FeCo and FeCoV Alloys," *J. Electrochem. Soc.* **150**, No. 3, C184–C188 (2003).
56. T. Osaka, T. Yokoshima, D. Shiga, K. Imai, and K. Takashima, "A High Moment CoFe Soft Magnetic Thin Film Prepared by Electrodeposition," *Electrochem. Solid-State Lett.* **6**, No. 4, C53–C55 (2003).
57. H. Xu, T. E. Dinan, E. I. Cooper, L. T. Romankiw, C. Bonhôte, and D. Miller, "Experimental Studies on Electrodeposition of CoFe Alloys," Paper No. 319, presented at the 199th Meeting of The Electrochemical Society, Washington, DC, 2001.
58. J. W. Chang, P. C. Andricacos, B. Petek, and L. T. Romankiw, "Electrodeposition of Soft CoFe Alloys," *Magnetic Materials, Processes and Devices*, L. T. Romankiw and D. A. Herman, Jr.,

Eds., **PV 90-8**, The Electrochemical Society Proceedings Series, Pennington, NJ, 1999, pp. 361–372.
59. C. F. Baes, Jr. and R. E. Mesmer, *The Hydrolysis of Cations*, Robert E. Krieger Publishing, Malabar, FL, 1986.
60. H. Deligianni and L. T. Romankiw, "*In Situ* Surface pH Measurement During Electrolysis Using a Rotating pH Electrode," *IBM J. Res. & Dev.* **37**, No. 2, 85–95 (1993).
61. H. Deligianni and L. T. Romankiw, "Effect of Near-Surface pH on Electrodeposition of Nickel," *Magnetic Materials, Processes and Devices*, L. T. Romankiw and D. A. Herman, Jr., Eds., **PV 90-8**, The Electrochemical Society Proceedings Series, Pennington, NJ, 1990, pp. 407–421.
62. M. Pourbaix, *Atlas of Electrochemical Equilibria in Aqueous Solutions*, Pergamon Press, New York, 1966.
63. C. Madore, M. Matlosz, and D. Landolt, "Experimental Investigation of the Primary and Secondary Current Distribution in a Rotating Cylinder Hull Cell," *J. Appl. Electrochem.* **22**, 1155–1160 (1992).
64. A. Brenner, *Electrodeposition of Alloys*, Vols. 1 and 2, Academic Press, Inc., New York, 1963.
65. H. Dahms and I. M. Croll, "The Anomalous Codeposition of Iron–Nickel Alloys," *J. Electrochem. Soc.* **112**, 771–775 (1965).
66. S. Hessami and C. W. Tobias, "A Mathematical Model for Anomalous Codeposition of Nickel–Iron on a Rotating Disk Electrode," *J. Electrochem. Soc.* **136**, 3611–3616 (1990).
67. Y. Hsu and J. Heidmann, "Inductance and Domain Configuration of Write Heads," *Digest of Technical Papers, International Magnetics Conference (INTERMAG)*, 1999.
68. H. Xu, J. Heidmann, and Y. Hsu, "Domain Studies of Electroplated High Moment CoFe and $Ni_{45}Fe_{55}$ on Test Structures," *Magnetic Materials, Processes and Devices VII and Electrodeposition of Alloys*, S. Krongelb, L. T. Romankiw, J.-W. Chang, Y. Kitamoto, J. W. Judy, C. Bonhôte, G. Zangari, and W. Schwarzacher, Eds., **PV 2002-27**, The Electrochemical Society Proceedings Series, Pennington, NJ, 2003, pp. 307–318.
69. D. A. Thompson and J. S. Best, "The Future of Magnetic Data Storage Technology," *IBM J. Res. & Dev.* **44**, No. 3, 311–321 (2000).
70. C.-W. Chen, *Magnetism and Metallurgy of Soft Magnetic Materials*, Dover Publications, New York, 1986, pp. 197–203.
71. D. Bagayoko and J. Callaway, "Lattice-Parameter Dependence of Ferromagnetism in bcc and fcc Iron," *Phys. Rev. B* **28**, No. 10, 5419–5422 (1983).
72. F. J. Himpsel, "Exchange Splitting of Epitaxial fcc Fe/Cu(100) Versus bcc Fe/Ag(100)," *Phys. Rev. Lett.* **67**, No. 17, 2363–2366 (1991).
73. W. A. A. Macedo, W. Keune, and E. D. Ellerbrock, "Magnetic Properties of Ultrathin Epitaxial fcc–Fe(001) Films on Cu(001) and Cu_3Au(001)," *J. Magn. Magn. Mater.* **93**, 552–556 (1991).
74. F. Pan, M. Zhang, and B. X. Liu, "Magnetic Properties of fcc Iron in Fe/fcc Metal Multilayers," *Thin Solid Films* **334**, 196–200 (1998).
75. F. J. Pinski, J. Staunton, B. L. Gyorffy, D. D. Johnson, and G. M. Stocks, "Ferromagnetism Versus Antiferromagnetism in Face-Centered-Cubic Iron," *Phys. Rev. Lett.* **56**, 2096–2099 (1986).
76. D. D. Johnson, F. J. Pinski, and J. B. Staunton, "The Slater–Pauling Curve: First Principles Calculations of the Moments of Fe_{1-c} Ni_c and V_{1-c} Fe_c," *J. Appl. Phys.* **61**, No. 8, 3715–3717 (1987).

Received September 10, 2004; accepted for publication November 2, 2004; Internet publication January 6, 2005

Emanuel I. Cooper *IBM Research Division, Thomas J. Watson Research Center, P.O. Box 218, Yorktown Heights, New York 10598 (eicooper@us.ibm.com)*. Dr. Cooper received a B.Sc. degree in 1975 and a Ph.D. degree in 1981, both in chemistry, from the Technion–Israel Institute of Technology. After a postdoctoral fellowship at Purdue University, in 1984 he joined the IBM Research Division, where he first worked in a variety of fields including ceramics and composites for packaging, high-T_c superconductors, ionic liquids, new analytical applications of pH titrations, and stabilization of peroxide-based process solutions. More recently he has studied electrodeposition of soft magnetic alloy films for data storage and MEMS applications, and plating of bismuth-containing alloys for thermoelectric and interconnect applications. He is currently working on issues related to copper electroprocessing. Dr. Cooper is a member of The Electrochemical Society and the American Chemical Society.

Christian Bonhôte *Hitachi Global Storage Technologies, San Jose Research Center, 650 Harry Road, San Jose, California 95120*. Dr. Bonhôte received his Ph.D. degree in materials science from the Swiss Federal Institute of Technology in Lausanne, Switzerland. His thesis work was in the field of composition-modulated nanolayers created by electrodeposition. After a few years in Switzerland working in the field of irradiation-assisted stress corrosion cracking of nuclear reactors, Dr. Bonhôte joined the IBM Thomas J. Watson Research Center in Yorktown Heights, New York, to work on the electrodeposition of ultrahigh-moment magnetic alloys for recording heads. During his postdoctoral assignment at IBM Yorktown, Dr. Bonhôte received a temporary assignment at the IBM Almaden Research Center to work on electroplating of CoNiFe. He later joined the Advanced Head Development and Nanostructures group at the IBM Almaden Research Center as an electroplating expert. Dr. Bonhôte is currently working on the improvement of the electrodeposition of magnetic materials (CoFe alloys), material structure and property characterization, and protection against corrosion.

Juergen Heidmann *Hitachi Global Storage Technologies, San Jose Research Center, 650 Harry Road, San Jose, California 95120 (juergen.heidmann@hitachigst.com)*. Dr. Heidmann is a Senior Engineer/Scientist in the Advanced Magnetic Recording Characterization Department at the Hitachi–Global Storage Technologies San Jose Research Center. After receiving a Ph.D. degree from Wuppertal University, Germany, in electrical engineering/materials science, he spent two years at Wuppertal University conducting research and teaching in the field of micromagnetics. In 1989 he was granted an IBM Postdoctoral Fellowship to conduct research on recording media at the IBM San Jose Research Center. He joined the IBM General Storage Division in San Jose in 1991. Dr. Heidmann received an IBM Technical Achievement Award for his development of an ultrahigh-speed time-domain scanning Kerr apparatus. He is the author or coauthor of more than 30 technical papers in the field of magnetic recording physics. He currently works on ultrafast magneto dynamics in recording heads and recording media.

Yimin Hsu *Hitachi Global Storage Technologies, 5600 Cottle Road, San Jose, California 95193 (yimin.hsu@hitachigst.com)*. Dr. Hsu is a Senior Engineer in the Head-Media Advanced Technology Department at Hitachi Global Storage Technologies in San Jose. After receiving a Ph.D. degree from the University of Minnesota in materials science in 1992, he worked at Headway Technologies, Inc. His work focused on design and characterization of dual-stripe MR heads and also noise and magnetic instability of MR heads. Subsequently he managed a recording physics group. In 1996 Dr. Hsu joined the IBM Almaden Research Center as a Research Staff

Member. He worked on magnetization reversal and high-speed switching of magnetic thin films and inductive write heads, as well as the design and characterization of high-density inductive write heads. Currently his work involves a perpendicular head project.

Philippe Kern *Swiss Federal Laboratories for Materials Testing and Research (EMPA), CH-3602 Thun, Switzerland (philippe.kern@empa.ch)*. Dr. Kern received a Ph.D. degree in materials science from the Swiss Federal Institute of Technology Lausanne (EPFL) in 2001. That same year he joined IBM at the Thomas J. Watson Research Center, Yorktown Heights, New York, as a Postdoctoral Fellow to work on the electroplating of CoFe high-moment material for thin-film write heads. In 2002 he returned to EPFL to work on electrochemical microstructuring of biomedical surfaces. Dr. Kern is at present head of the Micro/Nanopatterning Group within the Swiss Federal Laboratories for Materials Testing and Research. His current research activities include electrochemical functionalization of biomedical surfaces, electrodeposition of biomedical/bioactive coatings, and electrodeposition of novel alloys for MEMS.

John W. Lam *Hitachi Global Storage Technologies, San Jose Research Center, 650 Harry Road, San Jose, California 95120.* After receiving a B.S. degree in chemical engineering from San Jose State University in 2000, Mr. Lam worked in the materials research and development group of Hitachi Global Storage Technologies at the San Jose Research Center, where he focused on electrodeposition of soft magnetic materials. He is currently pursuing research on electrodeposition of new materials used in the fabrication of thin-film heads.

Murali Ramasubramanian *FormFactor Inc., 2140 Research Drive, Livermore, California 94550 (mramasubramanian@formfactor.com)*. Dr. Ramasubramanian is a Process Development Engineer at FormFactor Inc. He received a B.Tech. degree in chemical and electrochemical engineering from The Central Electrochemical Research Institute, India, in 1993, and a Ph.D. degree in chemical engineering from the University of South Carolina in 1998. He subsequently joined the IBM Thomas J. Watson Research Center as a postdoctoral researcher working on electrodeposited high-moment magnetic films. Dr. Ramasubramanian continued this work as a thin-film/electrodeposition process development engineer for the IBM Storage Technology Division in San Jose from 1999 to 2002, and for the Hitachi Global Storage Technologies process development group in 2003. His current work at FormFactor Inc. pertains to the research and development of novel electrodeposition processes for semiconductor and MEMS applications.

Neil Robertson *Hitachi Global Storage Technologies, San Jose Research Center, 650 Harry Road, San Jose, California 95120.* Dr. Robertson is a manager at Hitachi Global Storage Technologies. He manages the Advanced Head Development and Nanotechnology Department at the San Jose Research Division. He received his B.S. degree in chemical engineering in 1982 from Cornell University and his Ph.D. degree in chemical engineering in 1988 from UC Berkeley, where he worked on problems in high-temperature electrochemical engineering. He worked on advanced technology for magnetic recording heads for 14 years in the IBM Almaden Research Center and the IBM Storage Division. Dr. Robertson managed projects on head design, magnetic materials, and process integration for advanced heads. Major projects included IBM recording density demonstrations, the first integration of GMR spin-valve materials into a recording head, advanced tape heads, and the development of advanced electroplated write-head materials. A major thrust of his work has been the use of new materials, processes, and designs to improve magnetic recording performance. Dr. Robertson has 30 patents filed or pending as well as 25 external publications. He has received several internal IBM awards for his work. He is a member of The Electrochemical Society and the IEEE Magnetics Society.

Lubomyr T. Romankiw *IBM Research Division, Thomas J. Watson Research Center, P.O. Box 218, Yorktown Heights, New York 10598 (romankiw@us.ibm.com)*. Dr. Romankiw is an IBM Fellow in the Science and Technology Department at the IBM Thomas J. Watson Research Center. His specific areas of interest are electrochemical technology, magnetic materials, devices, microfabrication, and MEMS. He received a B.Sc. degree in chemical engineering in 1955 from the University of Alberta, and M.Sc. and Ph.D. degrees in metallurgy and materials science in 1962 from the Massachusetts Institute of Technology. Since joining IBM in 1962, he has worked on developing dry and electrochemical fabrication processes for magnetic thin-film heads, X-ray lithography masks, bubble memory devices, silicon integrated circuits, and electronic packages. Dr. Romankiw has authored or coauthored 57 patents, more than 160 technical papers and reports, and four book chapters; he was an organizer of eleven major symposia and an editor of ten ECS symposium proceedings volumes. He is a member of The Electrochemical Society, the AESF, the International Society of Electrochemistry, the IEEE, the Schevchenko Scientific Society, the Ukrainian Engineers Society, Sigma Xi, and Phi Lambda Upsilon. Dr. Romankiw has received seven IBM Outstanding Invention and Outstanding Contribution Awards and 26 IBM Invention Achievement Awards. In 1984, together with R. J. Von Gutfeld, he received the Research Award from the Electrodeposition Division of The Electrochemical Society. Dr. Romankiw was named IBM Fellow in 1986, member of the IBM Academy of Technology in 1987, and ECS Fellow in 1990; he was elected a member of the Academy of Engineering Sciences of Ukraine in 1992. He received the AESF Scientific Achievement Award in 1992, the ACS Distinguished Chemist of Westchester Award in 1993, and the Perkin Medal, also in 1993. He was awarded the Morris A. Liebman Award in 1994 and was named IEEE Fellow in 1996. In 2001 Dr. Romankiw was named Inventor of the Year by the New York IP Law Association. In 2003 he became an honorary member of the Schevchenko Scientific Society and The Electrochemical Society.

Hong Xu was a Research Engineer at the IBM Almaden Research Center between 1998 and 2002; she subsequently joined Hitachi Global Storage Technologies and worked there until 2003. She worked on the development of electroplating of high-magnetic-moment alloys for write heads. Ms. Xu also worked on thin-film characterization for read heads. She received her M.S. degree in chemical engineering in 1998.